Macrophages regulate gastrointestinal motility through complement component 1q

Mihir Pendse[1], Yun Li[1], Cristine N. Salinas[1], Gabriella Quinn[1], Nguyen Vo[1], Daniel C. Propheter[1], Chaitanya Dende[1], Alexander A. Crofts[1], Eugene Koo[1], Brian Hassell[1], Kelly A. Ruhn[1], Prithvi Raj[1], Yuuki Obata[1*], Lora V. Hooper[1,2*]

[1]Department of Immunology, The University of Texas Southwestern Medical Center, Dallas, TX 75390

[2]The Howard Hughes Medical Institute, The University of Texas Southwestern Medical Center, Dallas, TX 75390

***For correspondence:** yuuki.obata@utsouthwestern (YO), lora.hooper@utsouthwestern.edu (LVH)

ABSTRACT

Peristaltic movement of the intestine propels food down the length of the gastrointestinal tract to promote nutrient absorption. Interactions between intestinal macrophages and the enteric nervous system regulate gastrointestinal motility, yet we have an incomplete understanding of the molecular mediators of this crosstalk. Here we identify complement component 1q (C1q) as a macrophage product that regulates gut motility. Macrophages were the predominant source of C1q in the mouse intestine and most extraintestinal tissues. Although C1q mediates complement-mediated killing of bacteria in the bloodstream, we found that C1q was not essential for immune defense of the intestine. Instead, C1q-expressing macrophages were localized to the intestinal submucosal plexus where they closely associated with enteric neurons and expressed surface markers characteristic of nerve-adjacent macrophages in other tissues. Mice with a macrophage-specific deletion of *C1qa* showed changes in enteric neuronal gene expression, increased peristaltic activity, and accelerated intestinal transit. Our findings identify C1q as a key regulator of gastrointestinal motility and provide enhanced insight into the crosstalk between macrophages and the enteric nervous system.

INTRODUCTION

Peristalsis is the physical force that propels food through the intestine, promoting digestion and nutrient absorption. The gastrointestinal motility that underlies peristalsis is a complex process that requires coordination of the activity of smooth muscle cells by enteric neurons (Rao and Gershon, 2016). Recent studies have revealed that intestinal macrophages impact gastrointestinal motility by regulating the functions of enteric neurons and facilitating their interactions with smooth muscle cells (Muller et al., 2014; Matheis et al., 2020).

Macrophages carry out diverse functions in the intestine that vary according to their anatomic location. For example, macrophages that localize to the tissue located directly underneath the gut epithelium — known as the lamina propria — contribute to immune defense against pathogenic bacteria

27 (Gabanyi et al., 2016). A distinct group of macrophages localizes to the tissues located beneath the lamina
28 propria, between the circular and longitudinal muscle layers in the tissue region known as the muscularis
29 externa. These muscularis macrophages express genes that are distinct from lamina propria macrophages
30 (Gabanyi et al., 2016). They directly regulate the activity of smooth muscle cells (Luo et al., 2018) and
31 secrete soluble factors such as bone morphogenetic protein 2 (BMP2) that interact with the enteric neurons
32 that control smooth muscle activity (Muller et al., 2014). Muscularis macrophages thus play a key role in
33 regulating gut motility. However, our understanding of the molecular mechanisms by which these
34 macrophages regulate intestinal neuromuscular activity and gut motility remains limited.

35 C1q is a member of the defense collagen family that has distinct functions in immune defense and
36 nervous system development and function (Bossi et al., 2014; Casals et al., 2019; Shah et al., 2015; Thielens
37 et al., 2017). It is composed of six molecules each of C1qA, C1qB, and C1qC, forming a 410 kDa oligomer.
38 C1q circulates in the bloodstream, where it participates in immune defense against infection by recognizing
39 antibodies bound to invading bacteria. This binding interaction initiates the classical complement pathway,
40 which entails the recruitment and proteolytic processing of other complement components that rupture the
41 bacterial membrane and recruit phagocytic cells (Kishore and Reid, 2000; Noris and Remuzzi, 2013). C1q
42 is also produced by microglia (brain-resident macrophage-like cells) in the brain where it promotes the
43 pruning of neuronal synapses through an unclear mechanism (Hammond et al., 2020; Hong et al., 2016).
44 Consequently, C1q deficiency results in heightened synaptic connectivity in the central nervous system that
45 can lead to epilepsy (Chu et al., 2010).

46 C1q is also produced at barrier sites, such as the intestine, where encounters with commensal and
47 pathogenic microbes are frequent. However, little is known about the physiological role of C1q in barrier
48 tissues. Liver immune cells, including macrophages and dendritic cells, produce serum C1q; however the
49 cellular source of C1q in barrier tissues including the intestine remains unclear (Petry et al., 2001). Here,
50 we show that C1q is produced by macrophages that inhabit the submucosal plexus of the mouse intestine.
51 These C1q-expressing macrophages are located close to enteric neurons that have a known role in
52 controlling gut motility. Consistent with their nerve-adjacent localization, mice lacking macrophage C1q

53 exhibit altered expression of enteric neuronal genes, increased peristaltic activity, and accelerated
54 gastrointestinal motility. These findings identify C1q as a key mediator of a neuroimmune interaction that
55 regulates gut motility.
56
57
58 **RESULTS**
59 **C1q is expressed in intestinal macrophages**
60 Soluble defense collagens are an ancient, evolutionarily conserved family of antimicrobial proteins
61 with shared structural features including a *C*-terminal globular head and a collagen-like region (Casals et
62 al., 2019). Little is known about the function of defense collagens at mucosal barrier sites, where microbial
63 encounter is frequent. Our initial goal in this study was to identify soluble defense collagens that are
64 expressed by the mouse intestine and to assess their role in host defense. We therefore measured the
65 expression of 18 defense collagen genes in the mouse small intestine and colon by RNA sequencing (RNA-
66 seq). The most abundant soluble defense collagen transcripts in the small intestine and colon were those
67 encoding C1qA, C1qB, and C1qC (***Figure 1A; Figure 1 – figure supplement 1***).
68 Serum C1q is produced by liver dendritic cells, monocytes, and macrophages (El-Shamy et al.,
69 2018). However, the cellular source(s) of C1q in peripheral tissues including the intestine is unknown.
70 Quantitative PCR (qPCR) analysis of fluorescence-activated cell sorting (FACS)-sorted cell suspensions
71 recovered from the small intestines of wild-type C57BL/6 mice revealed that *C1qa*, *C1qb*, and *C1qc*
72 transcripts were most abundant in $CD45^+$ cells, which include all immune cells, as compared to $CD45^-$ cells,
73 which encompass epithelial cells and other non-immune cells (***Figure 1B***). Further, C1q transcripts and
74 protein were most abundant in $CD45^+$ cells recovered from the subepithelial compartment, which includes
75 both the lamina propria and muscularis, as compared to $CD45^+$ cells recovered from the intraepithelial
76 compartment of the small intestine (***Figure 1C and D***). Thus, C1q is expressed by immune cells located in
77 the subepithelial compartment of the intestine and is largely absent from epithelial cells and intraepithelial
78 immune cells.

To identify intestinal immune cells that expresse C1q, we further analyzed the subepithelial CD45$^+$ cell population by flow cytometry. Expression of C1q transcripts and protein was highest in CD11b$^+$MHCII$^+$F4/80^{hi} macrophages and was mostly absent from non-macrophage immune cells (***Figure 1E-H***). Thus, C1q is expressed by macrophages in the mouse small intestine.

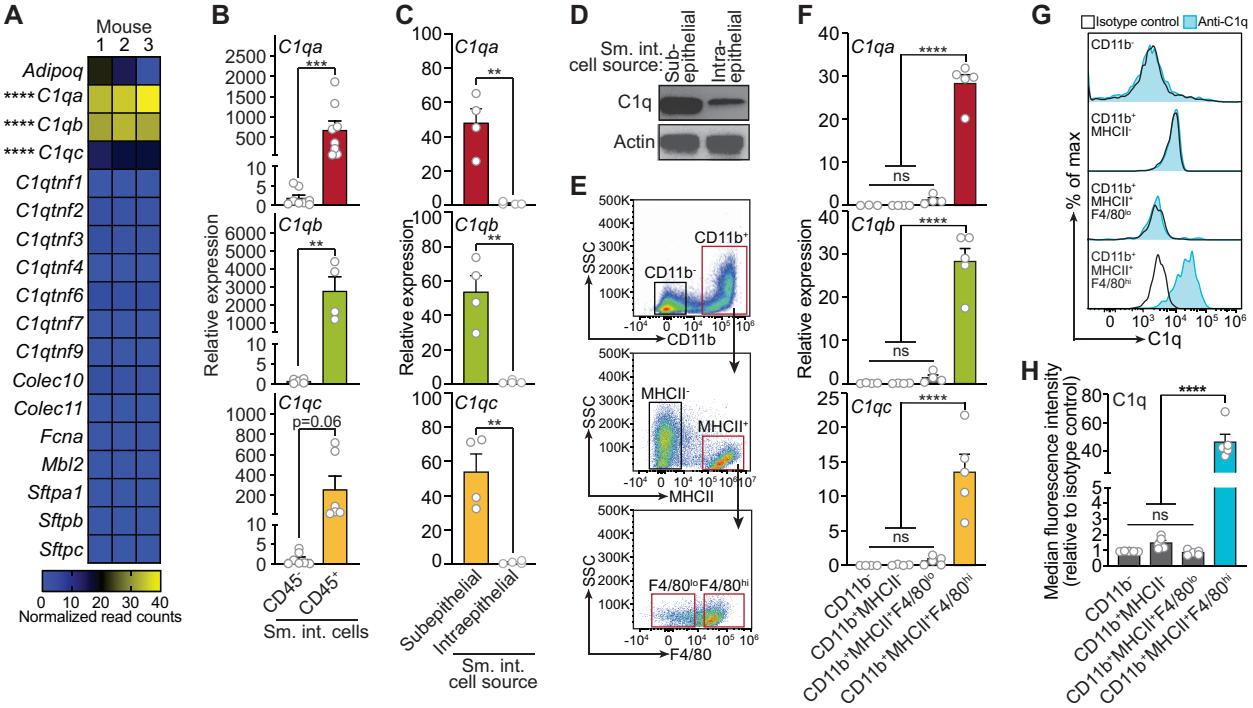

Figure 1. C1q is expressed by macrophages in the mouse small intestine.
(A) RNA-seq analysis of soluble defense collagen expression in the small intestines (ileum) of C57BL/6 mice. Data were adapted from a previously published RNA-seq analysis (Gattu et al., 2019). Data are available in the Gene Expression Omnibus repository under accession number GSE122471. Each column represents one mouse.
(B) qPCR measurement of *C1qa*, *C1qb*, and *C1qc* transcript abundance in CD45$^+$ and CD45$^-$ cells purified from mouse small intestines by flow cytometry. Each data point represents one mouse, and results are representative of two independent experiments.
(C) qPCR measurement of *C1qa*, *C1qb*, and *C1qc* transcript abundance in subepithelial and intraepithelial cells recovered from mouse small intestines. Each data point represents one mouse, and results are representative of three independent experiments.
(D) Representative immunoblot of subepithelial and intraepithelial cells recovered from mouse small intestines, with detection of C1q and actin (control). Each lane represents cells from one mouse and immunoblot is representative of three independent experiments.
(E) Flow cytometry gating strategy for analysis of mouse small intestinal cell suspensions in panels F, G, and H. Cells were pre-gated as live CD45$^+$ cells. SSC, side-scatter; MHCII, major histocompatibility complex II.
(F) qPCR measurement of *C1qa*, *C1qb*, and *C1qc* transcript abundance in cells isolated by flow cytometry from mouse small intestines as indicated in (E). Each data point represents cells pooled from three mice, and results are representative of three independent experiments.
(G) Flow cytometry analysis of intracellular C1q in small intestinal subepithelial cells identified as indicated in (E).
(H) Quantitation of flow cytometry analysis in (G). Each data point represents one mouse, and results are representative of two independent experiments.

Sm. int., mouse small intestine; Error bars represent SEM. **p<0.01; ***p<0.001; ****p<0.0001; ns, not significant by one way ANOVA (A,F) or two-tailed Student's t-test (B,C,H).

Figure supplement 1. C1q is expressed in the mouse colon.

Macrophages are the primary source of C1q in the mouse gastrointestinal tract

We next assessed whether macrophages are the primary source of C1q in the intestine by analyzing two mouse models. First, we depleted macrophages by injecting neutralizing antibodies directed against the receptor for colony stimulating factor 1 (CSF1R)(***Figure 2A***), which is required for the development of a subset of lamina propria macrophages (Bogunovic et al., 2009) and all muscularis macrophages (Muller et al., 2014). Antibody injection led to a >2-fold reduction in the number of macrophages recovered from the small intestine (***Figure 2B***), and a corresponding >2-fold reduction in small intestinal C1q gene expression **(*Figure 2C*)**, suggesting that macrophages are the primary source of intestinal C1q.

Second, we constructed a genetic model of C1q deficiency by crossing *C1qa*$^{fl/fl}$ mice (Fonseca et al., 2017) to mice carrying the *Lyz2-Cre* transgene (LysM-Cre mice), which is selectively expressed in myeloid cells including macrophages (***Figure 2D***). These mice, hereafter designated as *C1qa*$^{\Delta M\phi}$ mice, lacked C1q expression in intestinal macrophages (***Figure 2E and F***). Importantly, *C1qa*$^{\Delta M\phi}$ mice had markedly lower C1q expression in both the small intestine and colon (***Figure 2G***), indicating that macrophages are the main source of C1q in the intestine. Unexpectedly, the *C1qa*$^{\Delta M\phi}$ mice also lost *C1q* gene expression in the lung, skin, kidney, and liver (but not the brain), and C1q protein was undetectable in the serum (***Figure 2 – figure supplement 1***). These findings indicate that macrophages are the primary source of C1q in the intestine and suggest that LysM^{+} macrophages or macrophage-like cells are also the main source of C1q in most extraintestinal tissues and the bloodstream.

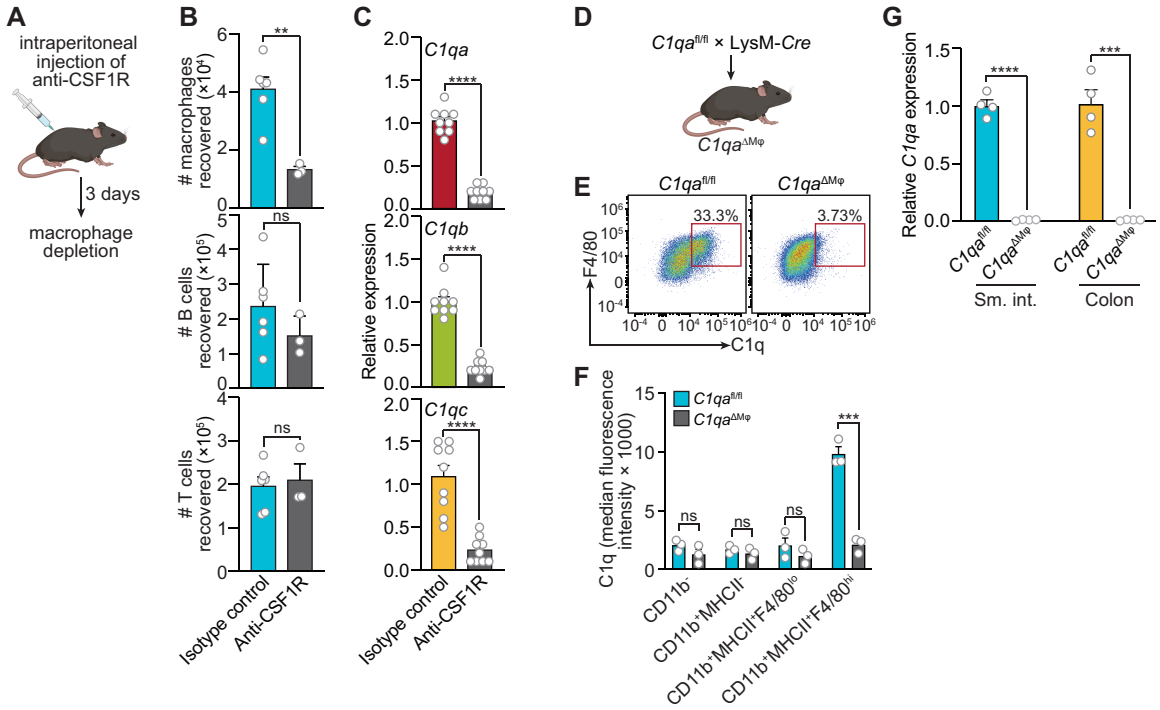

Figure 2. Macrophages are the primary source of C1q in the mouse gastrointestinal tract.
(A) Graphic showing selective depletion of macrophages in C57BL/6 mice by intraperitoneal injection of anti-CSF1R antibody. Control mice were injected with isotype-matched non-specific antibody. Mice were analyzed 72 hours after antibody injection. Panel was generated at Biorender.com.
(B) Representative flow cytometry analysis of mouse small intestines after intraperitoneal injection of anti-CSF1R or isotype control antibody. All cells were gated as live $CD45^+$. Macrophages were $MHCII^+$ $F4/80^{hi}$; B cells were $CD19^+$; T cells were $CD3^+$. Total small intestinal cell yields were $1.5 \times 10^6 \pm 4.9 \times 10^5$ cells.
(C) qPCR measurement of *C1qa*, *C1qb*, and *C1qc* transcript abundance in mouse small intestines after intraperitoneal injection of anti-CSF1R or rat IgG2a (isotype control). Each data point represents one mouse and results are pooled from two independent experiments.
(D) $C1qa^{fl/fl}$ mice were crossed with mice harboring a LysM-Cre transgene to generate mice having a macrophage-selective deletion of *C1qa* ($C1qa^{\Delta M\varphi}$ mice). Panel was generated at Biorender.com.
(E) Representative flow cytometry analysis of intracellular C1q expression in small intestinal macrophages from $C1qa^{fl/fl}$ and $C1qa^{\Delta M\varphi}$ mice. Mice were littermates from heterozygous crosses that remained co-housed. Cells were gated on live $CD45^+CD11b^+MHCII^+$.
(F) Quantitation of the flow cytometry analysis in (E). Each data point represents one mouse. Results are representative of two independent experiments.
(G) qPCR measurement of *C1qa* transcript abundance in the small intestines (sm. int.) and colons of $C1qa^{fl/fl}$ and $C1qa^{\Delta M\varphi}$ littermates. Each data point represents one mouse.

Error bars represent SEM. **p<0.01; ***p<0.001; ****p<0.0001; ns, not significant by two-tailed Student's t-test.

Figure supplement 1. C1q expression is lost systemically but preserved in the central nervous system of $C1qa^{\Delta M\varphi}$ mice.

158 ***C1qa*$^{\Delta M\varphi}$ mice do not show altered microbiota composition, barrier function, or resistance to enteric**
159 **infection**

160 The classical complement pathway is a well-studied host defense system that protects against
161 systemic pathogenic infection (Warren et al., 2002; Noris and Remuzzi, 2013). Circulating C1q activates
162 the complement pathway by binding to antibody-antigen complexes or to bacterial cell surface molecules,
163 and thus protects against systemic infection. We therefore assessed whether C1q promotes immune defense
164 of the intestine.

165 We first determined whether C1q exhibits characteristics of known intestinal antimicrobial
166 proteins, including induction by the intestinal microbiota and secretion into the gut lumen. *C1qa* was
167 expressed at similar levels in the small intestines of germ-free and conventionally-raised mice (***Figure 3A***),
168 suggesting that *C1q* expression is not induced by the gut microbiota. This contrasted with *Reg3g*, encoding
169 the antimicrobial protein REG3G (Cash et al., 2006), which was expressed at a >2-fold higher level in
170 conventional as compared to germ-free mice (***Figure 3A***). Additionally, in contrast to REG3G, C1q was
171 not detected in the gut lumen of either conventional or germ-free mice (***Figure 3B***). *C1qa* expression was
172 also not markedly altered by oral infection with the intestinal pathogenic bacterial species *Salmonella*
173 Typhimurium (***Figure 3C***). These data indicate that C1q is not induced by the gut microbiota or by the
174 bacterial pathogen *S.* Typhimurium, in contrast to other antibacterial proteins.

175 We next assessed whether C1q regulates the composition of the gut microbiota. 16*S* rRNA gene
176 sequencing analysis of the fecal microbiotas of *C1qa*$^{fl/fl}$ and *C1qa*$^{\Delta M\phi}$ mice showed that the microbiota
177 composition was not appreciably altered in the absence of macrophage C1q (***Figure 3D***). We also
178 challenged *C1qa*$^{fl/fl}$ and *C1qa*$^{\Delta M\phi}$ mice with dextran sulfate sodium (DSS), which damages the colonic
179 epithelium and exposes underlying tissues to the commensal microbiota. However, the sensitivity of the
180 *C1qa*$^{\Delta M\phi}$ mice to DSS was similar to that of their *C1qa*$^{fl/fl}$ littermates as assessed by change in body weight
181 (***Figure 3E***). There was also no change in intestinal paracellular permeability in *C1qa*$^{\Delta M\phi}$ mice as measured

182 by oral administration of FITC-dextran (***Figure 3F***). These results suggest that macrophage C1q does not
183 substantially impact gut microbiota composition or intestinal epithelial barrier function.

184 To determine whether C1q protects against enteric infection we conducted oral infection
185 experiments with the enteric pathogen *Citrobacter rodentium*. We chose *C. rodentium* as our model
186 organism for two reasons. First, *C. rodentium* is a non-disseminating pathogen, allowing us to test
187 specifically for C1q's role in intestinal infection. Second, *C. rodentium* clearance depends on
188 immunoglobulins and complement component C3 (Belzer et al., 2011). Because C1q is bactericidal in
189 concert with C3 and immunoglobulins, we predicted that $C1qa^{\Delta M\phi}$ mice would be more susceptible to *C.*
190 *rodentium* infection. However, $C1qa^{\Delta M\phi}$ mice cleared *C. rodentium* similarly to their $C1qa^{fl/fl}$ littermates,
191 indicating that C1q is dispensable for defense against *C. rodentium* infection (***Figure 3G***).

192 We also did not observe marked alterations in immunity in the absence of C1q. Comparison of
193 cytokine transcript abundance in the small intestines of $C1qa^{fl/fl}$ and $C1qa^{\Delta M\phi}$ littermates revealed no
194 statistically significant differences in cytokine expression (***Figure 3H***). There were also no statistically
195 significant differences in the percentages or absolute numbers of various T cell subsets, including $T_{helper}1$
196 (T_H1), T_H2, T_H17, and regulatory T (T_{reg}) cells between $C1qa^{fl/fl}$ and $C1qa^{\Delta M\phi}$ mice (***Figure 3I; Figure 3 –***
197 ***figure supplement 1***). Although total B cell numbers trended lower in $C1qa^{\Delta M\phi}$ mice, the difference was
198 not statistically significant (***Figure 3I; Figure 3 – figure supplement 2***). There were also no statistically
199 significant differences in the percentages or absolute numbers of total plasma cells (***Figure 3I; Figure 3 –***
200 ***figure supplement 2***), IgA^+ plasma cells (***Figure 3I; Figure 3 – figure supplement 2***), myeloid cells
201 (***Figure 3I; Figure 3 – figure supplement 3***), or innate lymphoid cells (***Figure 3I; Figure 3 – figure***
202 ***supplement 4***) when comparing $C1qa^{fl/fl}$ and $C1qa^{\Delta M\phi}$ mice. These results suggest that the absence of
203 macrophage C1q has little impact on intestinal immunity. Altogether, our findings suggest that C1q does
204 not participate substantially in intestinal immune defense and thus might have an intestinal function that is
205 independent of its canonical role in activating the classical complement pathway.
206

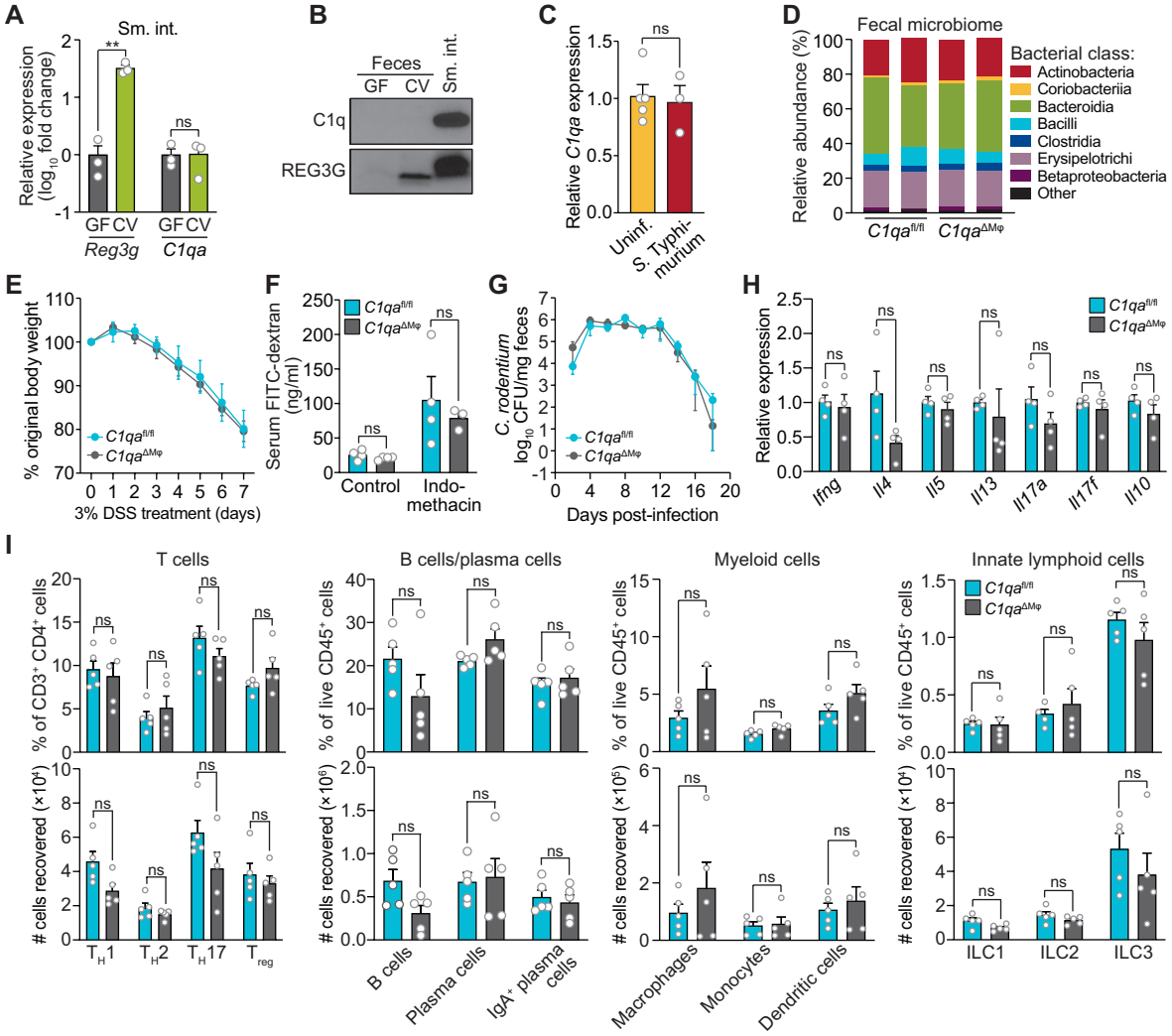

Figure 3. *C1qa*$^{\Delta M\varphi}$ mice do not show altered microbiota composition, barrier function, or resistance to enteric infection.

(A) Small intestinal *C1qa* expression is not induced by the intestinal microbiota. qPCR measurement of *Reg3g* and *C1qa* transcript abundances in the small intestines of germ free (GF) and conventional (CV) C57BL/6 mice. Each data point represents one mouse and results are representative of two independent experiments.

(B) C1q is not detected in the mouse intestinal lumen or feces. Representative immunoblot of an ammonium sulfate precipitation of intestinal lumenal contents and feces from germ-free and conventional mice with detection of C1q. C1q in small intestinal tissue (sm. int.) is shown for comparison at right. REG3G was detected as a control, as it is secreted into the intestinal lumen of conventional mice (Cash et al., 2006). Each lane represents multiple mice pooled (n = 5 and 9 for germ-free and conventional, respectively) and the immunoblot is representative of three independent experiments.

(C) C1q gene expression is not altered by enteric infection with *S.* Typhimurium. qPCR measurement of *C1qa* transcript abundance in small intestinal tissue after oral inoculation of mice with 10^9 colony forming units of *S.* Typhimurium strain SL1344. Each data point represents one mouse, and results are representative of two independent experiments.

(D) Intestinal microbiota composition is not altered in *C1qa*$^{\Delta M\varphi}$ mice. Phylogenetic analysis of 16*S* rRNA gene sequences from fecal pellets collected from *C1qa*$^{fl/fl}$ and *C1qa*$^{\Delta M\varphi}$ littermates. Operational taxonomic units with an average of 100 reads and populations greater than or equal to 1% were included in the graphical analysis. Each bar represents one mouse. Data are available from the Sequence Read Archive under BioProject ID PRJNA793870.

(E) *C1qa*$^{\Delta M\varphi}$ mice do not show altered susceptibility to dextran sulfate sodium (DSS)-induced colitis. Mice were provided with 3% DSS in drinking water and body weights were monitored for 7 days. n = 4 and 6 for *C1qa*$^{fl/fl}$ and

C1qa$^{\Delta M\varphi}$ littermates, respectively. Error bars represent SEM. Differences at each time point were not significant by two-tailed Student's t-test.

(F) *C1qa*$^{\Delta M\varphi}$ mice do not show altered intestinal permeability. To measure intestinal permeability, *C1qa*$^{fl/fl}$ and *C1qa*$^{\Delta M\varphi}$ littermates were gavaged with FITC-dextran, and serum FITC-dextran levels were determined by fluorescence microplate assay against a FITC-dextran standard curve. Indomethacin induces intestinal damage in mice and was used as a positive control.

(G) Time course of fecal *C. rodentium* burden following oral gavage of *C1qa*$^{fl/fl}$ and *C1qa*$^{\Delta M\varphi}$ mice with 5×10^8 colony forming units (CFU) of *C. rodentium*. n = 5 and 5 for *C1qa*$^{fl/fl}$ and $^{C1qa\Delta M\varphi}$ littermates, respectively. Error bars represent SEM. Differences at each time point were not significant by two-tailed Student's t-test.

(H) qPCR measurement of cytokine transcript abundances in the small intestines of *C1qa*$^{fl/fl}$ and *C1qa*$^{\Delta M\varphi}$ littermates. Error bars represent SEM. Statistics were performed with two-tailed Student's t-test.

(I) Flow cytometry analysis of small intestinal immune cell subsets from *C1qa*$^{fl/fl}$ and *C1qa*$^{\Delta M\varphi}$ littermates. Gating strategies are shown in Figure 3 - figure supplement 1 through 4. ILC, innate lymphoid cell. Total small intestinal cell yields were $8.8 \times 10^6 \pm 2.9 \times 10^6$ cells.

Error bars represent SEM. **p<0.01; ns, not significant by two-tailed Student's t-test.

Figure supplement 1. Flow cytometry gating strategy for comparison of T cell populations in *C1qa*$^{fl/fl}$ and *C1qa*$^{\Delta M\varphi}$ mice.

Figure supplement 2. Flow cytometry gating strategy for comparison of B cell and plasma cell populations in *C1qa*$^{fl/fl}$ and *C1qa*$^{\Delta M\varphi}$ mice.

Figure supplement 3. Flow cytometry gating strategy for comparison of myeloid cell populations in *C1qa*$^{fl/fl}$ and *C1qa*$^{\Delta M\varphi}$ mice.

Figure supplement 4. Flow cytometry gating strategy for comparison of innate lymphoid cell populations in *C1qa*$^{fl/fl}$ and *C1qa*$^{\Delta M\varphi}$ mice.

C1q-expressing gut macrophages are located near enteric neurons

Intestinal macrophages perform distinct functions depending on their anatomical location. Macrophages in the lamina propria protect against invasion by pathogenic microbes and promote tissue repair (Grainger et al., 2017). In contrast, macrophages that reside in deeper intestinal tissues, including the submucosal plexus and muscularis (***Figure 4A***), regulate enteric smooth muscle cells and neurons that drive gastrointestinal motility (De Schepper, Stakenborg, et al., 2018; De Schepper, Verheijden, et al., 2018).

Immunofluorescence analysis revealed that C1q was located primarily beneath the lamina propria, in a region consistent with the location of the submucosal plexus of the small intestine and colon (***Figure 4A and B***). C1q was detected in a diffuse pattern close to macrophages in *C1qa*$^{fl/fl}$ mice and was absent in *C1qa*$^{\Delta M\phi}$ mice (***Figure 4B***) despite the presence of similar overall numbers of CD169$^+$ macrophages (***Figure 4 – figure supplement 1***). Although we did not observe direct colocalization of C1q with CD169, a macrophage marker that selectively marks nerve-adjacent macrophages (Ural et al., 2020), the pattern

268 was consistent with prior observations of C1q deposition in the extracellular matrix in the arterial wall (Cao
269 et al., 2003)(***Figure 4B***).

270 We next assessed the location of C1q relative to enteric neurons in the mouse small intestine.
271 Detection of the neuronal marker βIII tubulin (TUBB3) revealed the presence of two distinct layers of
272 enteric neurons: one just beneath the lamina propria that was consistent with the location of the submucosal
273 plexus, and one in the muscularis that was consistent with the location of the myenteric plexus (***Figure 4C***).
274 Immunofluorescence detection of C1q alongside TUBB3 revealed that C1q was located within an average
275 of ~5 μm of the nearest $TUBB3^+$ enteric neurons in the submucosal plexus and was largely absent from the
276 myenteric plexus (***Figure 4C***). Thus, C1q-producing gut macrophages are located close to enteric neurons
277 in the submucosal plexus.

278 C1q-producing intestinal macrophages exhibited several characteristics of nerve-adjacent
279 macrophages in other tissues. First, microglia in the central nervous system and nerve-adjacent
280 macrophages in peripheral tissues, such as the lung, are enriched for C1q gene expression (Fonseca et al.,
281 2017; Ural et al., 2020). This is consistent with our observations of C1q expression in nerve-adjacent
282 intestinal macrophages located in the submucosal plexus (***Figure 4C***). Second, nerve-adjacent macrophages
283 depend on a CSF1-CSF1R signaling axis for their maintenance and are therefore sensitive to anti-CSF1R
284 antibody-mediated depletion (Muller et al., 2014). Thus, our finding that anti-CSF1R administration
285 depleted C1q-expressing intestinal macrophages is consistent with their location near enteric neurons
286 (***Figure 2A-C***). Third, C1q-expressing intestinal macrophages showed elevated expression of Arginase 1,
287 CD169, and TREM2 (triggering receptor expressed on myeloid cells 2)(***Figure 4D***), which are enriched on
288 macrophages with known neuromodulatory functions (Colonna, 2003; Paloneva et al., 2002; Ural et al.,
289 2020). Thus, C1q-expressing intestinal macrophages are located near enteric neurons and exhibit
290 phenotypes characteristic of nerve-adjacent macrophages in other tissues.

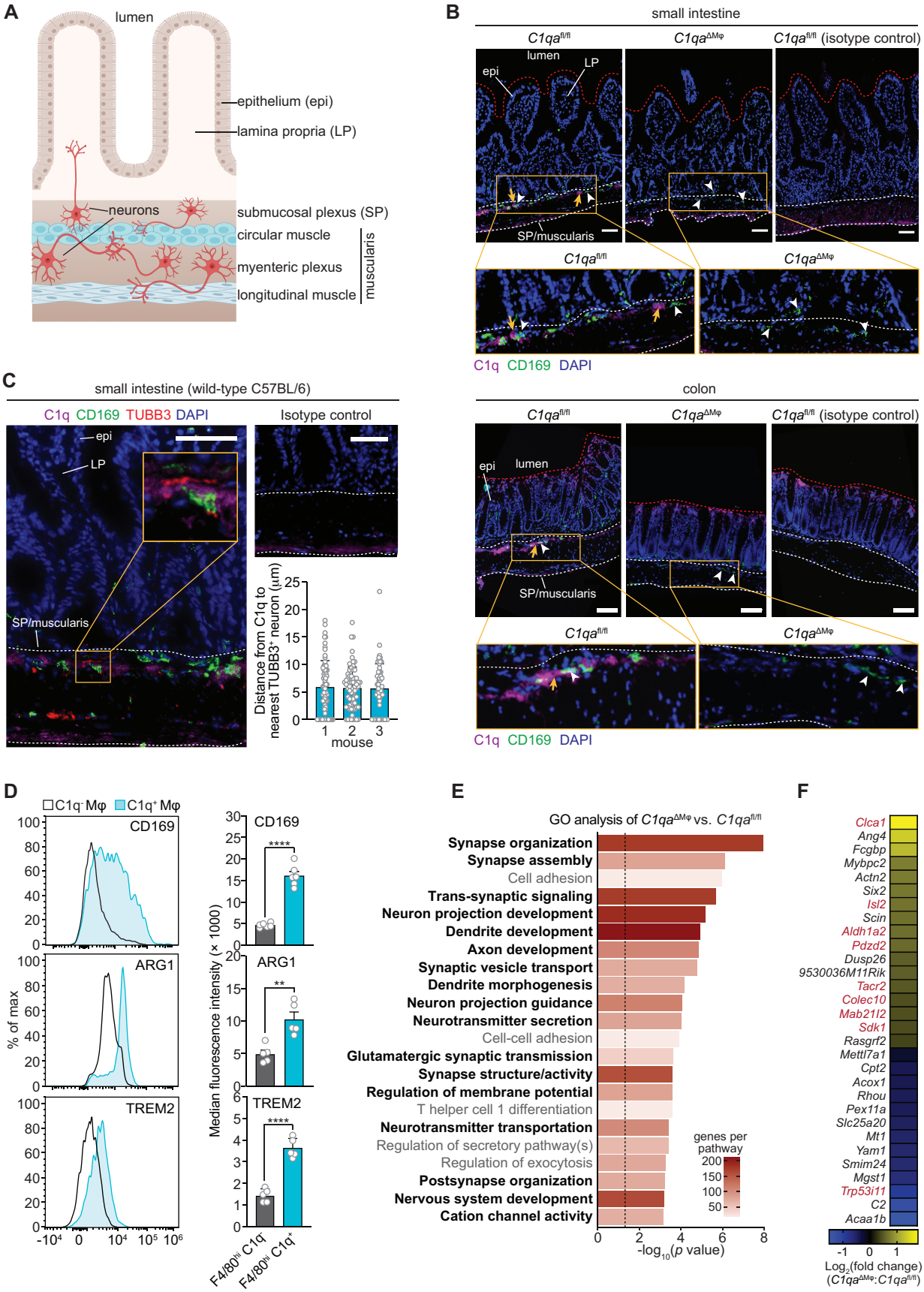
A
lumen
epithelium (epi)
lamina propria (LP)
neurons
submucosal plexus (SP)
circular muscle
myenteric plexus
longitudinal muscle
muscularis
B
small intestine
C1qa fl/fl
C1qa ΔMφ
C1qa fl/fl (isotype control)
epi
lumen
LP
SP/muscularis
C1q CD169 DAPI
C
small intestine (wild-type C57BL/6)
C1q CD169 TUBB3 DAPI
Isotype control
epi
LP
SP/muscularis
Distance from C1q to nearest TUBB3+ neuron (μm)
mouse
colon
D
C1q- Mφ
C1q+ Mφ
CD169
ARG1
TREM2
% of max
Median fluorescence intensity (× 1000)
F4/80hi C1q-
F4/80hi C1q+
E
GO analysis of C1qa ΔMφ vs. C1qa fl/fl
Synapse organization
Synapse assembly
Cell adhesion
Trans-synaptic signaling
Neuron projection development
Dendrite development
Axon development
Synaptic vesicle transport
Dendrite morphogenesis
Neuron projection guidance
Neurotransmitter secretion
Cell-cell adhesion
Glutamatergic synaptic transmission
Synapse structure/activity
Regulation of membrane potential
T helper cell 1 differentiation
Neurotransmitter transportation
Regulation of secretory pathway(s)
Regulation of exocytosis
Postsynapse organization
Nervous system development
Cation channel activity
genes per pathway
-log10(p value)
F
Clca1
Ang4
Fcgbp
Mybpc2
Actn2
Six2
Isl2
Scin
Aldh1a2
Pdzd2
Dusp26
9530036M11Rik
Tacr2
Colec10
Mab21l2
Sdk1
Rasgrf2
Mettl7a1
Cpt2
Acox1
Rhou
Pex11a
Slc25a20
Mt1
Yam1
Smim24
Mgst1
Trp53i11
C2
Acaa1b
Log2(fold change) (C1qa ΔMφ:C1qa fl/fl)

Figure 4. C1q-expressing macrophages are closely associated with neurons in the mouse intestine.
(A) Graphic depicting the muscularis of the mouse small intestine. The lumen, epithelium (epi), lamina propria (LP), submucosal plexus (SP), and distinct anatomical regions of the muscularis are indicated. Created at Biorender.com.
(B) Immunofluorescence detection of C1q (violet) and macrophages marked with CD169 (green) in the small intestine and colon of *C1qa*$^{fl/fl}$ and *C1qa*$^{\Delta M\varphi}$ littermates. Nuclei were detected with 4',6-diamidino-2-phenylindole (DAPI; blue). Detection with isotype control antibodies on *C1qa*$^{fl/fl}$ small intestines is shown at right. Anti-rat IgG AlexaFluor 488 and streptavidin-Cy5 were used as secondary stains for CD169 and C1q respectively. The intestinal surface is denoted with a red dotted line and the gut lumen, epithelium, and lamina propria are indicated. The approximate region encompassing the submucosal plexus and the muscularis is denoted with two white dotted lines. Examples of C1q^{+} areas are indicated with yellow arrows and examples of CD169^{+} macrophages are indicated with white arrowheads. Note that the violet staining near the bottom of the muscularis is non-specific, as indicated by its presence in the isotype control image. Images are representative of three independent experiments. Scale bars = 50 μm.
(C) Immunofluorescence detection of C1q (violet), macrophages marked with CD169 (green) and neurons marked with TUBB3 (red) in the small intestines of wild-type C57BL/6 mice. Nuclei are detected with DAPI (blue). The epithelium, lamina propria are indicated. The approximate region encompassing the submucosal plexus and the muscularis is denoted with two white dotted lines. The expanded image area delineated by a yellow square shows an example of the close association between C1q and TUBB3^{+} neurons. Images are representative of images captured from three mice. Anti-rat IgG AlexaFluor 488, anti-rabbit IgG AlexaFluor 594, and streptavidin-Cy5 were used as secondary stains for CD169, TUBB3, and C1q respectively, and an isotype control image is shown at upper right. Scale bars = 50 μm. Lower right panel: Distances between C1q^{+} areas and the nearest TUBB3^{+} neurons were measured in images captured from three mice. Each data point represents one measurement and measurements were made on 10 to 15 microscopic fields for each mouse (71, 70, and 57 total measurements, respectively).
(D) Flow cytometry analysis of CD169, Arginase 1, and TREM2 on C1q^{-} and C1q^{+} macrophages recovered from the small intestines of wild-type C57BL/6 mice. Median fluorescence intensities from multiple mice are quantified in the panels at right. Each data point represents one mouse (n=5-6 mice), and results are representative of two independent experiments. Error bars represent SEM. **$p<0.01$; ****$p<0.0001$ by two-tailed Student's t-test.
(E) Colonic longitudinal muscle myenteric plexus was acquired from *C1qa*$^{\Delta M\varphi}$ and *C1qa*$^{fl/fl}$ littermates. RNA-seq was performed, and annotated gene ontology (GO) biological processes were assigned to genes that were differentially expressed in *C1qa*$^{\Delta M\varphi}$ mice when compared to their *C1qa*$^{fl/fl}$ littermates. GO biological processes associated with neurons are in bold type. The dotted line indicates the cutoff for statistical significance. Five mice per group were analyzed as pooled biological replicates. Data are available from the Sequence Read Archive under BioProject ID PRJNA793870.
(F) The colonic longitudinal muscle myenteric plexus of *C1qa*$^{\Delta M\varphi}$ mice has a transcriptional profile like that of mice with a gastrointestinal motility disorder. RNA-seq was performed on the colonic longitudinal muscle-myenteric plexus from five *C1qa*$^{fl/fl}$ and five *C1qa*$^{\Delta M\varphi}$ littermates. Genes that were differentially expressed are represented in a heatmap that depicts $\log_2$(fold change). Genes that also showed altered expression in the TashT mouse line, which is a model of human Hirschsprung's disease (Bergeron et al., 2015), are indicated in red. Statistical significance of overlap between differentially expressed genes in *C1qa*$^{\Delta M\varphi}$ and TashT mice was determined by Fisher's exact test ($p = 0.0032$).

Figure supplement 1. Similar numbers of CD169^{+} macrophages are recovered from the small intestines of *C1qa*$^{\Delta M\varphi}$ and *C1qa*$^{fl/fl}$ littermates.

C1qa$^{\Delta M\phi}$ mice have altered gastrointestinal motility

Macrophages engage in crosstalk with the enteric nervous system and regulate functions, including gastrointestinal motility, that depend on the enteric nervous system (Muller et al., 2014). This crosstalk involves the exchange of specific proteins such as bone morphogenetic protein 2 (BMP2) (Muller et al., 2014). Given that C1q^{+} macrophages phenotypically resemble peripheral nerve-adjacent macrophages and

339 reside near enteric neurons, we postulated that macrophage-derived C1q might also regulate enteric nervous
340 system function.

341 As an initial test of this idea, we performed RNA-seq on the colonic longitudinal muscle-myenteric
342 plexus from *C1qa*$^{\Delta M\phi}$ and *C1qa*$^{fl/fl}$ littermates and then conducted unbiased Gene Set Enrichment Analysis.
343 Of the 22 biological pathways that were enriched in *C1qa*$^{\Delta M\phi}$ mice, 17 were related to neuronal development
344 or function, including synapse organization, dendrite development, and neurotransmitter secretion (***Figure***
345 ***4E***). 30 genes were differentially expressed when comparing the muscle-myenteric plexus of *C1qa*$^{\Delta M\phi}$ and
346 *C1qa*$^{fl/fl}$ mice (***Figure 4F***). These included genes with known roles in regulating neuronal activity (*Dusp26*),
347 synaptic transmission (*Rasgrf2*), and neuropeptide signaling (*Tacr2*) (Mao et al., 2017; Schwechter et al.,
348 2013; Yang et al., 2017). We also compared the list of genes differentially expressed in the *C1qa*$^{\Delta M\phi}$ mice
349 to those differentially expressed in the *TashT* mouse line. This line contains an insertional mutation that
350 leads to dysregulated gut motility comparable to Hirschsprung's disease, a human genetic disorder resulting
351 in incomplete development of the enteric nervous system (Bergeron et al., 2015). There was a statistically
352 significant overlap in the transcriptional changes in the colonic longitudinal muscle-myenteric plexus of
353 *C1qa*$^{\Delta M\phi}$ mice and *TashT* mice (***Figure 4F***). Together, these results suggest that macrophage C1q impacts
354 enteric nervous system gene expression and function.

355 Efficient coordination of gastrointestinal motility is necessary for proper digestion, nutrient
356 absorption, and excretion. Given that muscularis macrophages regulate enteric nervous system functions
357 that govern gastrointestinal motility (Muller et al., 2014), we assessed whether macrophage C1q impacts
358 gut motility. We first tested this idea by measuring gut transit time using the nonabsorbable dye carmine
359 red. *C1qa*$^{\Delta M\phi}$ and *C1qa*$^{fl/fl}$ littermates were gavaged with the dye and the time to first appearance of the dye
360 in the feces was recorded. Transit times were decreased in *C1qa*$^{\Delta M\phi}$ mice relative to their *C1qa*$^{fl/fl}$
361 littermates, indicating accelerated gut motility (***Figure 5A***). This was not due to a change in the lengths of
362 either the small intestine or the colon, which were unaltered in the *C1qa*$^{\Delta M\phi}$ mice (***Figure 5B***). By contrast,
363 gut transit time was unaltered in *C3*$^{-/-}$ mice, suggesting that macrophage C1q impacts gut motility

364 independent of its canonical function in the classical complement pathway (***Figure 5A***). Accelerated transit
365 was also observed in the small intestines of *C1qa*$^{\Delta M\phi}$ mice as assessed by rhodamine dye transit assay
366 (***Figure 5C***). We then conducted *ex vivo* colonic peristaltic recordings and observed that the colons of
367 *C1qa*$^{\Delta M\phi}$ mice exhibited greater neuromuscular activity as compared to *C1qa*$^{fl/fl}$ littermates (***Figure 5D;***
368 ***Figure 5 – figure supplement 1 and 2***). This indicated that the colons of *C1qa*$^{\Delta M\phi}$ mice maintained
369 increased peristaltic activity compared to their *C1qa*$^{fl/fl}$ littermates even in the absence of gut-extrinsic
370 signals. Finally, we directly assessed colonic motility by bead expulsion assay and found that *C1qa*$^{\Delta M\phi}$ mice
371 had accelerated colonic transit *in vivo* (***Figure 5E***). Thus, the absence of macrophage C1q increases
372 peristaltic activity and accelerates gut transit, indicating that macrophage C1q regulates gastrointestinal
373 motility.
374

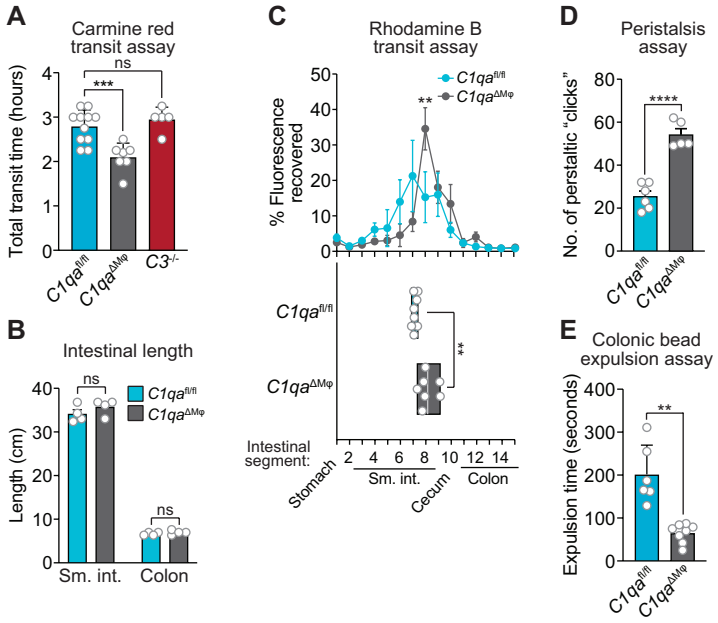

375 **Figure 5. *C1qa*$^{\Delta M\varphi}$ mice have altered gastrointestinal motility.**
376 **(A)** Measurement of total intestinal transit time in *C1qa*$^{fl/fl}$ and *C1qa*$^{\Delta M\varphi}$ littermates and *C3*$^{-/-}$ mice. Mice were gavaged
377 with 100 µl of carmine red (5% (w/v in 1.5% methylcellulose). Fecal pellets were collected every 15 minutes and
378 transit time was recorded when the dye was first observed in the feces. Each data point represents one mouse and the
379 results are pooled from five independent experiments.
380 **(B)** Intestinal tract length is not altered in *C1qa*$^{\Delta M\varphi}$ mice. Small intestines and colons from *C1qa*$^{fl/fl}$ and *C1qa*$^{\Delta M\varphi}$
381 littermates were excised and measured. Each data point represents one mouse.

382 **(C)** Transit of rhodamine B-dextran through the intestines of *C1qa*$^{fl/fl}$ and *C1qa*$^{\Delta M\varphi}$ littermates. Mice were sacrificed
383 90 minutes after gavage with rhodamine B-dextran. The intestines were divided into 16 segments, the rhodamine B
384 fluorescence was measured in each segment (top panel), and the geometric center of the fluorescence was determined
385 for each mouse (bottom panel). Each data point represents one mouse and the results were pooled from four
386 independent experiments.
387 **(D)** Quantification of *ex vivo* colonic peristalsis recordings. Peristaltic "clicks" were identified as terminally-oriented
388 waves of colonic muscle contraction. Each data point represents one mouse and the results are pooled from three
389 independent experiments.
390 **(E)** Colonic motility was measured by determining the expulsion time of a glass bead inserted intrarectally into
391 *C1qa*$^{fl/fl}$ and *C1qa*$^{\Delta M\varphi}$ littermates. Each data point represents one mouse and the results are representative of three
392 independent experiments.
393
394 sm. int., small intestine. Error bars represent SEM. **p<0.01; ***p<0.001; ns, not significant by two-tailed Student's
395 t-test.
396
397 **Figure supplements 1 and 2.** *Ex vivo* video recordings of colonic peristalsis in *C1qa*$^{fl/fl}$ and *C1qa*$^{\Delta M\varphi}$ littermates.
398

399

400 **DISCUSSION**

401 Here, we have identified a role for C1q in regulating gastrointestinal motility. We discovered that
402 nerve-adjacent macrophages are the primary source of C1q in the mouse intestine and that macrophage C1q
403 regulates enteric neuronal gene expression and gastrointestinal transit time. Our findings reveal a previously
404 unappreciated function for C1q in the intestine and help to illuminate the molecular basis for macrophage-
405 mediated control of gut motility.

406 Our study identifies macrophages as the main source of C1q in the mouse small intestine and colon.
407 Both transient antibody-mediated depletion of macrophages and *in vivo* deletion of the *C1qa* gene from
408 macrophages led to a marked reduction in intestinal *C1q* expression. The *C1qa*$^{\Delta M\phi}$ mice also lacked C1q in
409 the circulation, indicating that LysM^{+} macrophages or macrophage-like cells are also the source of
410 circulating C1q in the absence of infection. This enhances findings from prior studies indicating that
411 monocytes, macrophages, and immature dendritic cells are the main sources of C1q in the bloodstream (El-
412 Shamy et al., 2018). Importantly, the *C1qa*$^{\Delta M\phi}$ mice retained C1q expression in the brain, allowing us to
413 analyze the effects of C1q deficiency without possible confounding effects on the central nervous system.

414 C1q has two known physiological functions that are distinct and vary according to tissue context.
415 C1q was originally discovered as having a role in the classical complement pathway, which tags and
416 destroys invading microbes (Noris and Remuzzi, 2013; Schifferli et al., 1986). Circulating C1q binds to

417 invading microorganisms and recruits additional proteins that assemble into the membrane attack complex
418 (MAC) (Kishore and Reid, 2000). C1q-mediated MAC formation has been primarily described in the
419 bloodstream, where the necessary accessory proteins are present at high levels (Davis et al., 1979).
420 However, C1q is also expressed in the absence of infection in tissues such as the brain, where it regulates
421 neuronal development and function (Kouser et al., 2015; van Schaarenburg et al., 2016).

422 Our findings suggest that C1q does not play a central role in immune defense of the intestine. First,
423 we found that intestinal C1q expression was not induced by gut commensals or pathogens and was not
424 deposited into the gut lumen. Second, C1q deficiency did not markedly alter gut microbiota composition or
425 the course of disease after DSS treatment. There were also no major changes in cytokine expression or
426 numbers and frequencies of intestinal immune cells that would indicate dysregulated interactions with the
427 microbiota. Third, C1q was not required for clearance of *C. rodentium*, a non-disseminating enteric
428 pathogen whose clearance requires antigen-specific IgG and complement component 3 (C3) (Belzer et al.,
429 2011). Although we cannot rule out a role for C1q in immune defense against other intestinal pathogens,
430 these findings suggest that C1q is not essential for intestinal immune defense in mice.

431 Instead, our results indicate that C1q influences enteric nervous system function and regulates
432 intestinal motility. First, most C1q-expressing macrophages were localized to the intestinal submucosal
433 plexus and were largely absent from the lamina propria. Second, C1q-expressing intestinal macrophages
434 were located close to submucosal plexus neurons and expressed cell surface markers like those expressed
435 by nerve-adjacent C1q-expressing macrophages in the lung (Ural et al., 2020). Third, macrophage-specific
436 deletion of *C1qa* altered enteric neuronal gene expression. Finally, consistent with the altered neuronal gene
437 expression, macrophage-specific *C1qa* deletion altered gastrointestinal motility in both the small and large
438 intestine. Thus, our results suggest that the function of C1q in the intestine is similar to its function in the
439 brain, where it regulates the development and function of neurons (Kouser et al., 2015; van Schaarenburg
440 et al., 2016).

441 A function for macrophage C1q in intestinal motility adds to the growing understanding of how gut
442 macrophages regulate intestinal peristalsis. Prior work has shown that CSF1R^{+} macrophages selectively

443 localize to the muscularis of the mouse intestine (Muller et al., 2014; Gabanyi et al., 2016). These
444 macrophages secrete BMP2, which activates enteric neurons that regulate colonic muscle contraction and
445 thus colonic motility (Muller et al., 2014). We found that depletion of CSF1R^{+} macrophages reduces
446 intestinal C1q expression, and that macrophage-specific deletion of *C1qa* alters enteric neuronal gene
447 expression and gut motility. Thus, our findings suggest that C1q is a key component of the macrophage-
448 enteric nervous system axis.

449 An important remaining question concerns the molecular mechanism by which C1q regulates gut
450 motility. One possibility is that C1q shapes microbiota composition which, in turn, impacts gut motility.
451 This idea is suggested by studies in zebrafish showing that a deficiency in intestinal macrophages leads to
452 altered gut microbiota composition relative to wild-type zebrafish (Earley et al., 2018). Other studies in
453 zebrafish and mice have shown that severe defects in enteric nervous system development produce changes
454 in gut microbiota composition that are linked to dysregulated gut motility (Rolig et al., 2017; Johnson et
455 al., 2018). However, we did not observe marked changes in the composition of the gut microbiota in
456 *C1qa*$^{\Delta M\phi}$ mice, arguing against a central role for the microbiota in C1q-mediated regulation of gut motility.
457 A second possibility is that the absence of C1q leads to immunological defects that alter gut transit time.
458 This idea is consistent with studies showing that T cell cytokines can influence gastrointestinal motility
459 (Akiho et al., 2011). However, this seems unlikely given the lack of pronounced immunological
460 abnormalities in the intestines of *C1qa*$^{\Delta M\phi}$ mice.

461 A third possibility is that C1q interacts directly with enteric neurons or glial cells. Like
462 macrophage-produced BMP2 (Muller et al., 2014), C1q might bind to specific receptors on neurons to
463 regulate their activity. In support of this idea, mouse enteric neurons express *Adgrb1*, which encodes BAI1
464 (Obata et al., 2020), a known C1q receptor on human neural stem cells (Benavente et al., 2020). Other
465 studies have suggested that C1q functions as a signaling effector on immune cells and neurons (Benoit &
466 Tenner, 2011; Ling et al., 2018). Macrophages have also been reported to restrain neurogenesis in the
467 enteric nervous system through phagocytosis of apoptotic neurons (Kulkarni et al., 2017). Given that C1q

468 can opsonize dying host cells (Botto et al., 1998; Korb and Ahearn, 1997), C1q could regulate enteric
469 nervous system function by tagging apoptotic neurons for elimination. It is also possible that C1q acts
470 directly on enteric smooth muscle cells that regulate gut motility. Although we cannot rule out this
471 possibility, our transcriptional profile of the colonic myenteric plexus of *C1qa*$^{\Delta M\phi}$ mice suggests that most
472 of the transcriptional changes were associated with neurons.

473 Our findings on intestinal C1q have implications for human intestinal disease. Indeed, single cell
474 RNA-seq analysis shows that macrophages recovered from the human intestinal muscularis selectively
475 express *C1q* when compared to lamina propria macrophages (Domanska et al., 2022). Dysregulated
476 peristalsis is a characteristic of irritable bowel syndrome (Vrees et al., 2002) and is present in a subset of
477 inflammatory bowel disease patients (Bassotti et al., 2014). Our finding that macrophage C1q regulates gut
478 motility could suggest new strategies to prevent or treat these diseases. Additionally, most humans with
479 C1q deficiency develop systemic lupus erythematosus (SLE). Since C1q can target cellular debris for
480 phagocytosis, it is thought that C1q deficiency results in increased exposure of self-antigen to the immune
481 system, thereby reducing immune tolerance and causing autoimmune disease (Macedo and Isaac, 2016).
482 Furthermore, roughly 42.5% of SLE patients report gastrointestinal symptoms that range from acute
483 abdominal pain to chronic intestinal obstruction (Fawzy et al., 2016; Tian and Zhang, 2010). The exact
484 cause of these symptoms is unclear. Given that C1q deficiency is strongly correlated with SLE in humans
485 and alters gut motility in mice, we suggest that C1q could be a therapeutic target for SLE patients that
486 present with chronic constipation or other forms of dysregulated intestinal motility.

487

488 **MATERIALS AND METHODS**

489 **Key Resources Table**

Reagent type (species) or resource	Designation	Source or reference	Identifiers	Additional information
strain, strain background (*Mus musculus*)	*C1qa*$^{fl/fl}$; B6(SJL)-C1qa$^{tm1c(EUCOMM)Wtsi}$/TennJ	Jackson Laboratory; Fonseca et al., 2017	Stock #031261	
strain, strain background (*Mus musculus*)	LysM-Cre; B6.129P2-Lyz2$^{tm1(cre)Ifo}$/J	Jackson Laboratory; Claussen et al., 1999	Stock #004781	

Reagent type (species) or resource	Designation	Source or reference	Identifiers	Additional information
strain, strain background (*Mus musculus*)	*C1qa*$^{\Delta M\phi}$	this paper		Generated by crossing *C1qa*$^{fl/fl}$ mice with LysM-Cre mice
strain, strain background (*Mus musculus*)	*C3*$^{-/-}$; B6.129S4-C3^{tm1Crr}/J	Jackson Laboratory; Wessels et al., 1995	Stock #029661	
strain, strain background (*Mus musculus*)	Germ-free C57BL/6J mice	UT Southwestern Gnotobiotics Core Facility		
strain, strain background (*Salmonella enterica*)	*Salmonella enterica* subsp. enterica serovar Typhimurium strain SL1344	Dr. Vanessa Sperandio; Eichelberg and Galan, 1999		
strain, strain background (*Citrobacter rodentium*)	*Citrobacter rodentium* strain DBS100	ATCC	Strain# 51459	
antibody	Anti-Actin HRP (rabbit monoclonal)	Cell Signaling	Clone: 13E5	Immunoblot (1:5000)
antibody	Anti-ARG1 (sheep monoclonal)	R&D Systems	Clone: P05089	Flow (1:100)
antibody	Anti-B220 (rat monoclonal)	ThermoFisher	Clone: RA3-6B2	Flow (1:500)
antibody	Anti-C1q (rat monoclonal)	Cedarlane Laboratories	Clone: RmC7H8	Flow (1:50)
antibody	Anti-C1q (rabbit polyclonal)	ThermoFisher	Cat# PA5-29586	Immunoblot (1:500)
antibody	Anti-C1q-biotin (mouse monoclonal)	Abcam	Clone: JL1	ELISA (1:1000); Immunofluorescence (1:100)
antibody	Anti-CD3 (rat monoclonal)	ThermoFisher	Clone: 17A2	Flow (1:200)
antibody	Anti-CD4 (rat monoclonal)	BioLegend	Clone: GK1.5	Flow (1:500)
antibody	Anti-CD11b (rat monoclonal)	ThermoFisher	Clone: M1/70	Flow (1:200)
antibody	Anti-CD11c (Armenian hamster monoclonal)	ThermoFisher	Clone: N418	Flow (1:500)
antibody	Anti-CD16/32 (rat monoclonal)	BioLegend	Clone: 93	Fc receptor block (1:1000)
antibody	Anti-CD19 (rat monoclonal)	BioLegend	Clone: 1D3	Flow (1:500)
antibody	Anti-CD45 (rat monoclonal)	BioLegend	Clone: 30-F11	Flow (1:500)
antibody	Anti-CD90.2 (rat monoclonal)	BioLegend	Clone: 30-H12	Flow (1:500)
antibody	Anti-CD169 (rat monoclonal)	BioLegend	Clone: 3D6.112	Flow (1:200)
antibody	Anti-CD169 (rat monoclonal)	Abcam	Clone: 3D6.112	Immunofluorescence (1:200)
antibody	Anti-CSF1R (rat monoclonal)	Bio X Cell	Cat# AFS98	Macrophage depletion (dosage)
antibody	Anti-F4/80	BioLegend	Clone: BM8	Flow (1:100)
antibody	Anti-FoxP3 (rat monoclonal)	ThermoFisher	Clone: FJK-16s	Flow (1:50)
antibody	Anti-GATA3 (mouse monoclonal)	BD Biosciences	Clone: L50-823	Flow (1:50)
antibody	Anti-IgA (rat monoclonal)	ThermoFisher	Clone: 11-44-2	Flow (1:50)
antibody	Anti-LY6C	BioLegend	Clone: RB6-8C5	Flow (1:500)
antibody	Anti-MHCII	Thermo	Clone: M5/114.15.2	Flow (1:500)
antibody	Anti-REG3G antiserum (rabbit)	Cash et al., 2006; antiserum generated by Pacific Biosciences		Immunoblot (dilution)
antibody	Anti-RORγt	ThermoFisher	Clone: AFKJS-9	Flow (1:50)
antibody	Anti-T-BET	BioLegend	Clone: 4B10	Flow (1:50)
antibody	Anti-TREM2	R&D Systems	Clone: 237920	Flow (1:200)
antibody	Anti-TUBB3	Abcam	Cat# ab18207	Immunofluorescence (1:200)
antibody	Goat anti-rabbit IgG HRP conjugate	Abcam	Cat# ab6721	Immunoblot (1:5000)
antibody	secondary antibodies - AlexaFluor 488/594/647	Invitrogen		Immunofluorescence (1:400)

Reagent type (species) or resource	Designation	Source or reference	Identifiers	Additional information
antibody	mouse IgG1	Abcam	Cat# ab18443	ELISA (10 μg/ml)
antibody	Rat IgG2a	ThermoFisher	Clone: 2A3	Isotype control for anti-CSF1R macrophage depletion
antibody	Rat IgG1 PE isotype control	Cedarlane Laboratories	Cat# CLCR104	Flow (1:50)
sequence-based reagent	mouse *C1qa* TaqMan assay	ThermoFisher	Assay ID: Mm00432142_m1	
sequence-based reagent	mouse *C1qb* TaqMan assay	ThermoFisher	Assay ID: Mm01179619_m1	
sequence-based reagent	mouse *C1qc* TaqMan assay	ThermoFisher	Assay ID: Mm00776126_m1	
sequence-based reagent	mouse *Reg3g* TaqMan assay	ThermoFisher	Assay ID: Mm00441127_m1	
sequence-based reagent	mouse *Ifng* TaqMan assay	ThermoFisher	Assay ID: Mm01168134_m1	
sequence-based reagent	mouse *Il4* TaqMan assay	ThermoFisher	Assay ID: Mm00445259_m1	
sequence-based reagent	mouse *IL5* TaqMan assay	ThermoFisher	Assay ID: Mm00439646_m1	
sequence-based reagent	mouse *Il10* TaqMan assay	ThermoFisher	Assay ID: Mm01288386_m1	
sequence-based reagent	mouse *Il13* TaqMan assay	ThermoFisher	Assay ID: Mm00434204_m1	
sequence-based reagent	mouse *Il17a* TaqMan assay	ThermoFisher	Assay ID: Mm00439618_m1	
sequence-based reagent	mouse *Il17f* TaqMan assay	ThermoFisher	Assay ID: Mm00521423_m1	
sequence-based reagent	mouse 18*S* gene TaqMan assay	ThermoFisher	Assay ID: Mm03928990_g1	
sequence-based reagent	bacterial 16*S* V3 - rRNA gene forward primer	ThermoFisher; (Klindworth et al., 2013)	16*S* rRNA gene sequencing	5'-TCGTCGGCAGCGTCAGATGTGTATAAGAGACAGCCTACGGGNGGCWGCAG-3′
sequence-based reagent	bacterial 16*S* v4 - rRNA gene reverse primer	ThermoFisher; Klindworth et al., 2013	16*S* rRNA gene sequencing	5′-GTCTCGTGGGCTCGGAGATGTGTATAAGAGACAGGACTACHVGGGTATCTAATCC-3′
peptide, recombinant protein	recombinant mouse C1q	Complementech	Cat# M099	
commercial assay or kit	FOXP3/Transcription Factor Fixation/Permeabilization Buffer Set	ThermoFisher	Cat# 00-5523-00	
commercial assay or kit	MMLV Reverse Transcriptase Kit	ThermoFisher	Cat# 28025-021	
commercial assay or kit	PE300 (Paired end 300 bp) v3 kit	Illumina	Cat# MS-102-3001	
commercial assay or kit	RNeasy Universal Mini Kit	Qiagen	Cat# 73404	
commercial assay or kit	TaqMan Master Mix	ThermoFisher	Cat# 4369542	
commercial assay or kit	TruSeq RNA sample preparation kit	Illumina	Cat# RS-122-2001	
chemical compound, drug	Agencourt AmpureXP beads	Beckman Coulter Genomics	Cat# A63880	
chemical compound, drug	Carmine Red	Sigma	Cat# C1022-25G	
chemical compound, drug	Collagenase IV	Sigma	Cat# C5138-1G	
chemical compound, drug	Borosilicate glass beads (2mm)	Millipore Sigma	Cat# Z273627-1EA	
chemical compound, drug	Dextran sulfate sodium	Thomas Scientific	Cat# 216011090	
chemical compound, drug	DNase I	Sigma	Cat# DN25	
chemical compound, drug	Dispase II	Sigma	Cat# D4693-1G	
chemical compound, drug	FITC-dextran	Sigma	Cat# FD4-1g	
chemical compound, drug	Ghost 710	Tonbo Biosciences	Cat# 13-0871-T100	Flow cytometry viability dye

Reagent type (species) or resource	Designation	Source or reference	Identifiers	Additional information
chemical compound, drug	Methylcellulose	Sigma	Cat# M0262-100G	
chemical compound, drug	Nalidixic acid, sodium salt	Research Products International	Cat# N23100-25.0	
chemical compound, drug	Optimal Cutting Temperature Compound (OCT)	ThermoFisher	Cat# 23-730-571	
chemical compound, drug	Percoll Plus	GE Healthcare	Cat# GE17-0891-09	
chemical compound, drug	Protease inhibitors	Millipore Sigma	Cat# 11836153001	
chemical compound, drug	Rhodamine B-dextran	ThermoFisher	Cat# D1841	
chemical compound, drug	Streptavidin-Cy5	ThermoFisher	Cat# 434316	
chemical compound, drug	Streptavidin-HRP conjugate	Abcam	Cat# ab7403	ELISA
chemical compound, drug	VECTASHIELD Antifade Mounting Medium with DAPI	Vector Labs	Cat# H-1200-10	
software, algorithm	clusterProfiler			
software, algorithm	CLC Genomics Workbench			
software, algorithm	CLC Bio microbial genomics module			https:// digitalinsights.qiagen.com/plugins/clc-microbial-genomics-module/
software, algorithm	FlowJo			
software, algorithm	GraphPad PRISM	GraphPad Software	Version 7.0; RRID:SCR_002798	
software, algorithm	Igor Pro 9	WaveMetrics		
software, algorithm	Illumina Nextera Protocol	Illumina	Part # 15044223 Rev. B	
software, algorithm	ImageJ	National Institutes of Health		https://imagej.nih.gov/ij/
software, algorithm	NovoExpress	Agilent Technologies		
software, algorithm	PVCAM software	Teledyne Photometrics		
Other	Agilent 2100 Bioanalyzer	Agilent Technologies	G2939A	
Other	Amicon Ultra centrifugal filters	Millipore	Cat #UFC900324	
Other	BioRad ChemiDoc Touch System	BioRad	Cat# 1708370	
Other	CMOS camera	Teledyne Photometrics	MOMENT	
Other	Leica CM1950 (Cryostat)	Leica		
Other	FACSAria	BD Biosciences		
Other	Illumina MiSeq	Illumina	RRID:SCR_016379	
Other	Illumina NextSeq 500	Illumina		
Other	Keyence Fluorescence Microscope	Keyence	BZ-X800	
Other	NovoCyte 3005	Agilent Technologies		
Other	Organ bath chamber	Tokai Hit Co. (Japan)		
Other	Peristaltic pump	Gilson	MINIPULS3	
Other	QuantStudio 7 Flex Real-Time PCR System	Applied Biosystems	Cat #4485701	
Other	SpectraMax M5 plate reader	Molecular Devices		
Other	Zeiss Axio Imager M1 Microscope	Zeiss		

490

491 **Mice**

492 Wild-type C57BL/6J (Jackson Laboratory) and *C3*$^{-/-}$ mice (Jackson Laboratory; Wessels et al., 1995) were

493 bred and maintained in the SPF barrier facility at the University of Texas Southwestern Medical Center.

494 *C1qa*$^{\Delta M\phi}$ mice were generated by crossing *C1qa*$^{fl/fl}$ mice (Jackson Laboratory; Fonseca et al., 2017) with a
495 mouse expressing Cre recombinase controlled by the macrophage-specific mouse *Lyz2* promoter (LysM-
496 Cre mice; Jackson Laboratory; Clausen et al., 1999). Mice 8 to 12 weeks of age were used for all
497 experiments and cohoused littermates were used as controls. Both male and female mice were analyzed.
498 Germ-free C57BL/6J mice were bred and maintained in isolators at the University of Texas Southwestern
499 Medical Center. All procedures were performed in accordance with protocols approved by the Institutional
500 Animal Care and Use Committees (IACUC) of the UT Southwestern Medical Center.
501

502 **Quantitative polymerase chain reaction (qPCR)**

503 Tissue RNA was isolated using the RNeasy Universal Mini kit (Qiagen, Hilden, Germany). Cellular RNA
504 was isolated using the RNAqueous Micro kit (ThermoFisher). cDNA was generated from the purified RNA
505 using the M-MLV Reverse Transcriptase kit (ThermoFisher). qPCR analysis was performed using TaqMan
506 primer/probe sets and master mix (ThermoFisher) on a Quant-Studio 7 Flex Real-Time PCR System
507 (Applied Biosystems). Transcript abundances were normalized to 18*S* rRNA abundance. TaqMan probe
508 assay IDs are provided in the Key Resources table.
509

510 **Isolation and analysis of intestinal immune cells**

511 Lamina propria (LP) cells were isolated from the intestine using a published protocol (Yu et al., 2013; Yu
512 et al., 2014). Briefly, intestines were dissected from mice and Peyer's patches were removed. Intestines
513 were cut into small pieces and thoroughly washed with ice-cold phosphate-buffered saline (PBS) containing
514 5% fetal bovine serum (PBS-FBS). Epithelial cells were removed by incubating intestinal tissues in Hank's
515 buffered salt solution (HBSS) supplemented with 2 mM EDTA, followed by extensive washing with PBS-
516 FBS. Residual tissues were digested twice with Collagenase IV (Sigma), DNase I (Sigma) and Dispase (BD
517 Biosciences) for 45 minutes at 37°C with agitation. Cells were filtered through 70 μm cell strainers
518 (ThermoFisher) and applied onto a 40%:80% Percoll gradient (GE Healthcare). Subepithelial cell
519 populations were recovered at the interface of the 40% and 80% fractions. For small intestinal cell

520 suspensions, the epithelial fraction was kept and combined with enzymatically liberated subepithelial cells.
521 Cells were washed with 2 mM EDTA/3% FBS in PBS and Fc receptors were blocked with anti-CD16/32
522 (93). Cells were then stained with the viability dye Ghost 710 (Tonbo Biosciences) followed by antibodies
523 against cell surface markers including anti-CD45 (30-F11), anti-CD11b (M1/70), anti-MHCII
524 (M5/114.15.2), anti-F4/80 (BM8), anti-CD3 (17A2), anti-CD4 (GK1.5), anti-CD19 (1D3), anti-B220
525 (RA3-6B2), anti-CD11c (N418), anti-CD169 (3D6.112), anti-TREM2 (237920) and anti-LY6C (RB6-
526 8C5). Cells were fixed and permeabilized with the eBioscience FOXP3/Transcription Factor
527 Fixation/Permeabilization buffer set (ThermoFisher) and then subjected to intracellular staining with anti-
528 C1Q (RmC7H8), anti-FOXP3 (FJK-16s), anti-GATA3 (L50), anti-T-BET (4B10), anti-RORγ (AFKJS-9),
529 and anti-ARG1 (P05089). Cells were sorted using a FACSAria (BD Biosciences) or analyzed using a
530 NovoCyte 3005 (Agilent Technologies). Data were processed with FlowJo software (BD Biosciences) or
531 NovoExpress (Agilent Technologies).
532
533 **Macrophage depletion**
534 Anti-mouse CSF1R (ThermoFisher; AFS98) and rat IgG2a isotype control (ThermoFisher; 2A3) antibodies
535 were administered intraperitoneally at a concentration of 100 mg/kg. Mice were sacrificed 72 hours post-
536 injection and terminal ileum and colon were collected for qPCR analysis.
537
538 **Protein extraction from intestinal cells and feces**
539 To isolate proteins from intestinal cell suspensions, cell pellets were resuspended in 100 μl of RIPA Lysis
540 Buffer (ThermoFisher) supplemented with protease inhibitors (Millipore Sigma) and vortexed vigorously
541 every 5 minutes for 20 minutes. Lysates were cleared of cellular debris by centrifugation at 13000*g* for 5
542 minutes. To isolate proteins from the intestinal lumen, the entire gastrointestinal tract (from duodenum to
543 distal colon) was recovered from five wild-type C57BL/6J mice. The intestines were flushed with a total of
544 ~ 50 ml cold PBS containing protease inhibitors (Millipore Sigma, 11836153001). The flushes and fecal

545 pellets were homogenized by rotor and stator (TH Tissue Homogenizer; OMNI; TH01) and large particles
546 were centrifuged at 100*g* for 10 min at room temperature. The supernatants were carefully decanted and
547 centrifuged further at 3000*g* for 20 min at room temperature. The clarified supernatants were precipitated
548 with 40% ammonium sulfate overnight at 4°C. Precipitated protein was centrifuged at 3000*g* for 30 min at
549 4°C, then resuspended in cold 40% ammonium sulfate and centrifuged again. The pellets were resuspended
550 in room temperature PBS and allowed to mix for 10 min. Protein concentrations were determined by
551 Bradford assay (BioRad).
552
553 **Immunoblot**
554 50 μg of fecal protein or 25 μg of cellular protein was loaded onto a 4-20% gradient SDS-PAGE and
555 transferred to a PVDF membrane. Membranes were blocked in 5% nonfat dry milk in Tris-buffered saline
556 (TBS) with 0.1% Tween-20 and then incubated overnight with the following primary antibodies: anti-C1Q
557 (PA5-29586, ThermoFisher) and anti-actin (13E5, Cell Signaling). REG3G was detected by incubating
558 membranes with rabbit anti-REG3G antiserum (Cash et al., 2006). After washing, membranes were
559 incubated with goat anti-rabbit IgG HRP and then visualized with a BioRad ChemiDoc Touch system.
560
561 **Enzyme-linked immunosorbent assay (ELISA)**
562 Mouse C1q ELISA was performed as previously described (Petry et al., 2001). Briefly, microtiter plates
563 were coated overnight with mouse IgG1 and were then blocked with 5% BSA in PBS. Serum samples were
564 diluted 1:50 and plated for 1 hour at room temperature. After washing with 0.05% Tween-20 in PBS, bound
565 C1q was incubated with biotinylated anti-C1q antibody (JL1, Abcam). Biotinylated anti-C1q was detected
566 with a streptavidin-HRP conjugate (Abcam). Optical density was measured using a wavelength of 492 nm.
567 Plates were analyzed using a SpectraMax M5 microplate reader (Molecular Devices).
568
569
570

571 **Intestinal permeability assay**

572 Intestinal permeability assays were performed by treating mice with fluorescein isothiocyanate dextran
573 (FITC-dextran) by oral gavage. The non-steroidal anti-inflammatory drug (NSAID) indomethacin was
574 administered to mice as a positive control. For the experimental group, mice were treated with 190 µl 7%
575 dimethyl sulfoxide (DMSO) in PBS by oral gavage. For the positive control group, mice were treated with
576 190 µl indomethacin (1.5 mg/ml in 7% DMSO in PBS) by oral gavage. After 1 hour, all mice were treated
577 with 190 µl FITC-dextran (80 mg/ml in PBS) by oral gavage. Mice were sacrificed after 4 hours and sera
578 were collected. Serum samples were centrifuged for 20 minutes at 4°C at 800*g* and supernatants were
579 collected. Serum FITC-dextran levels were measured by a fluorescence microplate assay against a standard
580 curve using a Spectramax plate reader (Molecular Devices).

581

582 **Dextran sulfate sodium (DSS) treatment**

583 Age and sex-matched mice were provided with 3% dextran sulfate sodium (weight/volume) in autoclaved
584 drinking water for 7 days. Animal weight and health were monitored in accordance with institutional
585 IACUC guidelines.

586

587 ***Salmonella* Typhimurium infection**

588 To prepare bacteria for infection, *Salmonella enterica* serovar Typhimurium (SL1344) was cultured in
589 Luria-Bertani (LB) broth containing 50 µg/ml streptomycin in a shaking incubator at 37ºC (Eichelberg and
590 Galan, 1999). The overnight culture was diluted the next day and grown to mid-log phase (OD_{600} = 0.3-
591 0.5). *C1qa*$^{fl/fl}$ and *C1qa*$^{\Delta M\phi}$ littermates were inoculated intragastrically with 10^9 CFU. All mice were
592 sacrificed 24 hours later and small intestinal tissues were harvested for analysis.

593

594

595

596 ***Citrobacter rodentium* infection**

597 To prepare bacteria for infection, an overnight culture of *C. rodentium* (DBS100, ATCC) in LB broth
598 containing nalidixic acid (100 μg/ml) in a shaking incubator at 37°C. The overnight culture was diluted the
599 next day and grown to mid-log phase (OD_{600} = 0.4-0.6). Bacteria were pelleted, washed, and resuspended
600 in PBS. Sex-matched littermates were inoculated intragastrically with 5×10^8 CFU. Fecal pellets were
601 collected at a fixed time every 48 hours, homogenized in sterile PBS, diluted, and plated on LB agar with
602 nalidixic acid (100 μg/ml).

603

604 **Immunofluorescence analysis of mouse intestines**

605 Mouse small intestines and colons were flushed with PBS and embedded with Optimal Cutting Temperature
606 compound (OCT) (ThermoFisher). Sections were fixed in ice cold acetone, blocked with 1% BSA, 10%
607 FBS, 1% Triton X-100 in PBS, and then incubated overnight at 4ºC with the following antibodies: mouse
608 anti-C1q biotin (JL-1), rat anti-CD169 (3D6.112), and rabbit anti-TUBB3 (ab18207, Abcam). Slides were
609 then washed with PBS containing 0.2% Tween-20 (PBS-T) and incubated with donkey anti-rabbit
610 AlexaFluor 488, donkey anti-rat AlexaFluor 594, and Streptavidin-Cy5 (ThermoFisher) for 1 hour at room
611 temperature in the dark. Slides were then washed in PBS-T and mounted with DAPI-Fluoromount-G
612 (Southern Biotech). Mounted slides were cured overnight at 4ºC until imaging.

613

614 **RNA-seq analysis of colonic longitudinal muscle myenteric plexus**

615 The colonic longitudinal muscle-myenteric plexus was collected from five age and sex matched *C1qa*$^{fl/fl}$
616 and *C1qa*$^{\Delta M\phi}$ mice by manual dissection using a 2 mm metal probe (Fisher Scientific). RNA was isolated
617 using the RNeasy Mini kit according to the manufacturer's protocol (Qiagen). Quantity and quality of RNA
618 samples was assessed on an Agilent 2100 Bioanalyzer (Agilent Technologies). RNA-seq libraries were
619 prepared using the TruSeq RNA sample preparation kit (Illumina) according to the manufacturer's protocol.
620 Libraries were validated on an Agilent Bionalyzer 2100. Indexed libraries were sequenced on an Illumina

621 NextSeq550 for single-end 75 bp length reads. CLC Genomics Workbench 7 was used for bioinformatics
622 and statistical analysis of the sequencing data. The approach used by CLC Genomics Workbench is based
623 on a method developed previously (Mortazavi et al., 2008). To identify differentially enriched biological
624 pathways, all genes were ranked based on their $\log_2$fold-change and pathway enrichment was identified
625 using the R packages "clusterProfiler" and "msigdbr". For analysis of differentially expressed genes, gene
626 counts were analyzed using DESeq-2 and differentially expressed genes were defined as having an adjusted
627 p value <0.05. A Fisher's Exact Test was conducted to assess the overlap between differentially expressed
628 genes in *C1qa*$^{\Delta M\phi}$ mice and the TashT mouse (Bergeron et al., 2015).
629

630 **16*S* rRNA gene sequencing and analysis**

631 The hypervariable regions V3 and V4 of the bacterial 16*S* rRNA gene were prepared using the Illumina
632 Nextera protocol (Part # 15044223 Rev. B). An amplicon of 460 bp was amplified using the 16*S* Forward
633 Primer and 16*S* Reverse Primer as described in the manufacturer's protocol. Primer sequences are given in
634 the Key Resources Table. The PCR product was purified using Agencourt AmpureXP beads (Beckman
635 Coulter Genomics). Illumina adapter and barcode sequences were ligated to the amplicon to attach them to
636 the MiSeqDx flow cell and for multiplexing. Quality and quantity of each sequencing library were assessed
637 using Bioanalyzer and picogreen measurements, respectively. Libraries were loaded onto a MiSeqDX flow
638 cell and sequenced using the Paired End 300 (PE300) v3 kit. Raw fastq files were demultiplexed based on
639 unique barcodes and assessed for quality. Samples with more than 50,000 quality control pass sequencing
640 reads were used for downstream analysis. Taxonomic classification and operational taxonomic unit analysis
641 were done using the CLC Microbial Genomics Module. Individual sample reads were annotated with the
642 Greengene database and taxonomic features were assessed.
643

644 **Gastrointestinal motility assays**

645 Motility assays were adapted from previous studies (Luo et al., 2018; Maurer, 2016; Muller et al., 2014).
646 To determine transit time through the entire gastrointestinal tract, mice were fasted overnight and water

647 was removed 1 hour prior to the start of the experiment. Mice were then singly housed for 1 hour and then
648 gavaged with 100 µl of carmine red (5% weight/volume; Sigma) in 1.5% methylcellulose. Fecal pellets
649 were collected every 15 minutes and transit time was recorded when the dye was first observed in the feces.
650 For small intestinal motility measurements, mice were fasted overnight and then gavaged with 100
651 µl of rhodamine B-dextran (5 mg/ml; ThermoFisher) in 2% methylcellulose. After 90 minutes, mice were
652 sacrificed and their stomachs, small intestines, ceca, and colons were collected. Small intestines were cut
653 into 8 segments of equal length and colons were cut into 5 segments of equal length. Segments were cut
654 open lengthwise and vortexed in 1 ml PBS to release rhodamine B-dextran. Fluorescence was then
655 measured on a SpectraMax M5 microplate reader (Molecular Devices). The geometric center of the dye
656 was calculated as: GC = Σ (% of total fluorescent signal per segment × segment number). Relative
657 fluorescence per segment was calculated as: (fluorescence signal in segment / total fluorescence recovered)
658 x 100.
659 To measure colonic motility, mice were fasted overnight and lightly anesthetized with isoflurane.
660 A 2 mm glass bead was inserted 2 cm intrarectally using a 2 mm surgical probe. Mice were then returned
661 to empty cages and time to reappearance of the bead was recorded.
662 To account for potential circadian differences in gut motility, the time of day for the initiation of
663 all experiments was held constant.
664
665 ***Ex vivo* peristaltic imaging**
666 *Ex vivo* video imaging and analysis of colonic peristalsis was carried out as described previously (Obata et
667 al., 2020). Colons were dissected, flushed with sterile PBS, and pinned into an organ bath chamber (Tokai
668 Hit, Japan) filled with high glucose Dulbecco's Modified Eagle Medium (DMEM). DMEM was oxygenated
669 (95% O_2 and 5% CO_2), run through the chamber using a peristaltic pump (MINIPULS 3, Gilson) and kept
670 at 37°C. Colons were allowed to equilibrate to the organ chamber for 30 minutes before video recording.
671 Movies of colonic peristalsis were captured with a camera (MOMENT, Teledyne photometrics) using

672 PVCAM software (500ms time-lapse delay) over 15 minutes. Movies consist of 3000 sequential image
673 frames that were stitched together in ImageJ and analyzed at a rate of 7 frames per second.
674
675 **Statistical analysis**
676 Graphed data are presented as means ± standard error of the mean (SEM). Statistics were determined with
677 GraphPad Prism software. Statistical analyses were performed using two-tailed Student's t test when
678 comparing two groups, one way ANOVA when comparing multiple groups, and Fisher's exact test to assess
679 overlap between groups of differentially expressed genes. The statistical tests used are indicated in the
680 figure legends. *$P \leq 0.05$; **$P \leq 0.01$; ***$P \leq 0.001$; and ns, $P > 0.05$.
681
682
683 **ADDITIONAL INFORMATION**
684 **Acknowledgements**
685 We thank Shai Bel for assistance with immunofluorescence imaging experiments, the UT Southwestern
686 Genomics Core for assistance with RNA sequencing experiments, and the UT Southwestern Flow
687 Cytometry Core for assistance with flow cytometry experiments. *Citrobacter rodentium* strain DBS100
688 was a gift from Vanessa Sperandio. This work was supported by NIH grants R01 DK070855 (L.V.H.),
689 Welch Foundation Grant I-1874 (L.V.H.), the Walter M. and Helen D. Bader Center for Research on
690 Arthritis and Autoimmune Diseases (L.V.H.), and the Howard Hughes Medical Institute (L.V.H.). M.P.
691 and A.A.C. were supported by NIH T32 AI005284. E.K. was supported by NIH F31 DK126391. Y.O. is
692 the Nancy Cain Marcus and Jeffrey A. Marcus Scholar in Medical Research, in Honor of Dr. Bill S. Vowell.
693
694 **Competing interests:** The authors declare no competing interests.
695
696
697

698 **Author contributions**

699 Mihir Pendse, Conceptualization, Investigation, Data curation, Formal analysis, Methodology, Supervision,
700 Writing – original draft, Writing – review and editing; Yun Li, Investigation; Cristine N. Salinas,
701 Investigation; Gabriella Quinn, Data curation, Formal analysis; Daniel C. Propheter, Investigation, Writing
702 – review and editing; Chaitanya Dende, Investigation, Writing – review and editing; Alexander A. Crofts,
703 Data curation, Formal analysis; Eugene Koo, Methodology; Brian Hassell, Investigation; Kelly A. Ruhn,
704 Investigation; Prithvi Raj, Investigation, Data curation, Formal analysis; Yuuki Obata, Investigation,
705 Methodology, Writing – original draft, Writing – review and editing; Lora V. Hooper, Conceptualization,
706 Funding acquisition, Supervision, Writing – original draft, Writing – review and editing.

707

708 **Data availability**

709 16*S* rRNA gene sequencing data (***Figure 3D***) and RNA sequencing data (***Figure 4E and F; Figure 4 –***
710 ***figure supplement 2***) are available from the Sequence Read Archive under BioProject ID PRJNA793870.
711 All mouse strains used are available commercially.

712
713
714
715
716 **REFERENCES**
717
718

719 Akiho, H., Ihara, E., Motomura, Y., Nakamura, K. (2011). Cytokine-induced alterations of gastrointestinal
720 motility in gastrointestinal disorders. *World J Gastrointest Pathophysiol, 2*, 72-81.
721 https://doi.org/10.4291/wjgp.v2.i5.72
722
723 Bassotti, G., Antonelli, E., Villanacci, V., Salemme, M., Coppola, M., Annese, V. (2014). Gastrointestinal
724 motility disorders in inflammatory bowel diseases. *World J Gastroenterol, 20*, 37-44.
725 https://doi.org/10.3748/wjg.v20.i1.37
726
727 Belzer, C., Liu, Q., Carroll, M. C., Bry, L. (2011). The role of specific IgG and complement in combating
728 a primary mucosal infection of the gut epithelium. *Eur J Microbiol Immunol (Bp), 1*, 311-318.
729 https://doi.org/10.1556/EuJMI.1.2011.4.7
730
731 Benavente, F., Piltti, K.M., Hooshmand, M.J., Nava, A.A., Lakatos, A., Feld, B.G., Creasman, D., Gershon,
732 P.D., Anderson, A. (2020). Novel C1q receptor-mediated signaling controls neural stem cell behavior and
733 neurorepair. *eLife, 9*, e55732. https://doi.org/10.7554/eLife.55732

Benoit, M. E., Tenner, A. J. (2011). Complement protein C1q-mediated neuroprotection is correlated with regulation of neuronal gene and microRNA expression. *J Neurosci, 31*, 3459-3469. https://doi.org/10.1523/JNEUROSCI.3932-10.2011

Bergeron, K. F., Cardinal, T., Toure, A. M., Beland, M., Raiwet, D. L., Silversides, D. W., Pilon, N. (2015). Male-biased aganglionic megacolon in the TashT mouse line due to perturbation of silencer elements in a large gene desert of chromosome 10. *PLoS Genet, 11*, e1005093. https://doi.org/10.1371/journal.pgen.1005093

Bogunovic, M., Ginhoux, F., Helft, J., Shang, L., Hashimoto, D., Greter, M., Liu, K., Jakubzick, C., Ingersoll, M. A., Leboeuf, M., Stanley, E. R., Nussenzweig, M., Lira, S. A., Randolph, G. J., Merad, M. (2009). Origin of the lamina propria dendritic cell network. *Immunity, 31*, 513-525. https://doi.org/10.1016/j.immuni.2009.08.010

Bossi, F., Tripodo, C., Rizzi, L., Bulla, R., Agostinis, C., Guarnotta, C., Munaut, C., Baldassarre, G., Papa, G., Zorzet, S., Ghebrehiwet, B., Ling, G. S., Botto, M., Tedesco, F. (2014). C1q as a unique player in angiogenesis with therapeutic implication in wound healing. *Proc Natl Acad Sci U S A, 111*, 4209-4214. https://doi.org/10.1073/pnas.1311968111

Botto, M., Dell'Agnola, C., Bygrave, A. E., Thompson, E. M., Cook, H. T., Petry, F., Loos, M., Pandolfi, P. P., Walport, M. J. (1998). Homozygous C1q deficiency causes glomerulonephritis associated with multiple apoptotic bodies. *Nat Genet, 19*, 56-59. https://doi.org/10.1038/ng0598-56

Cao, W., Bobryshev, Y. V., Lord, R. S., Oakley, R. E., Lee, S. H., Lu, J. (2003). Dendritic cells in the arterial wall express C1q: potential significance in atherogenesis. *Cardiovasc Res, 60*, 175-186. https://doi.org/10.1016/s0008-6363(03)00345-6

Casals, C., Garcia-Fojeda, B., Minutti, C. M. (2019). Soluble defense collagens: Sweeping up immune threats. *Mol Immunol, 112*, 291-304. https://doi.org/10.1016/j.molimm.2019.06.007

Cash, H. L., Whitham, C. V., Behrendt, C. L., Hooper, L. V. (2006). Symbiotic bacteria direct expression of an intestinal bactericidal lectin. *Science, 313*, 1126-1130. https://doi.org/10.1126/science.1127119

Chu, Y., Jin, X., Parada, I., Pesic, A., Stevens, B., Barres, B., Prince, D. A. (2010). Enhanced synaptic connectivity and epilepsy in C1q knockout mice. *Proc Natl Acad Sci U S A, 107*, 7975-7980. https://doi.org/10.1073/pnas.0913449107

Clausen, B. E., Burkhardt, C., Reith, W., Renkawitz, R., Forster, I. (1999). Conditional gene targeting in macrophages and granulocytes using LysMcre mice. *Transgenic Res, 8*, 265-277. https://doi.org/10.1023/a:1008942828960

Colonna, M. (2003). TREMs in the immune system and beyond. *Nat Rev Immunol, 3*, 445-453. https://doi.org/10.1038/nri1106

Davis, C. A., Vallota, E. H., Forristal, J. (1979). Serum complement levels in infancy: age related changes. *Pediatr Res, 13*, 1043-1046. https://doi.org/10.1203/00006450-197909000-00019

De Schepper, S., Stakenborg, N., Matteoli, G., Verheijden, S., Boeckxstaens, G. E. (2018). Muscularis macrophages: Key players in intestinal homeostasis and disease. *Cell Immunol, 330*, 142-150. https://doi.org/10.1016/j.cellimm.2017.12.009

De Schepper, S., Verheijden, S., Aguilera-Lizarraga, J., Viola, M. F., Boesmans, W., Stakenborg, N., Voytyuk, I., Schmidt, I., Boeckx, B., Dierckx de Casterle, I., Baekelandt, V., Gonzalez Dominguez, E., Mack, M., Depoortere, I., De Strooper, B., Sprangers, B., Himmelreich, U., Soenen, S., Guilliams, M., Vanden Berghe, P., Jones, E., Lambrechts, D., Boeckxstaens, G. (2018). Self-maintaining gut macrophages are essential for intestinal homeostasis. *Cell, 175*, 400-415. https://doi.org/10.1016/j.cell.2018.07.048

Domanska, D., Majid, U., Karlsen, V.T., Merok, M.A., Beitnes, A.-C. R., Yaqub, S., Baekkevold, E.S., Jahnsen, F.L. (2022). Single-cell transcriptomic analysis of human colonic macrophages reveals niche-specific subsets. *J Exp Med, 219*, e20211846. https://doi.org/10.1084/jem.20211846

Earley, A.M., Graves, C.L., Shiau, C.E. (2018). Critical role for a subset of intestinal macrophages in shaping gut microbiota in adult zebrafish. *Cell Rep, 25*, 424-436. https://doi.org/10.1016/j.celrep.2018.09.025

Eichelberg, K., Galan, J. E. (1999). Differential regulation of Salmonella typhimurium type III secreted proteins by pathogenicity island 1 (SPI-1)-encoded transcriptional activators InvF and hilA. *Infect Immun, 67*, 4099-4105. https://doi.org/10.1128/IAI.67.8.4099-4105.1999

El-Shamy, A., Branch, A. D., Schiano, T. D., & Gorevic, P. D. (2018). The complement system and C1q in chronic hepatitis C virus infection and mixed cryoglobulinemia. *Front Immunol, 9*, 1001. https://doi.org/10.3389/fimmu.2018.01001

Fawzy, M., Edrees, A., Okasha, H., El Ashmaui, A., Ragab, G. (2016). Gastrointestinal manifestations in systemic lupus erythematosus. *Lupus, 25*, 1456-1462. https://doi.org/10.1177/0961203316642308

Fonseca, M. I., Chu, S. H., Hernandez, M. X., Fang, M. J., Modarresi, L., Selvan, P., MacGregor, G. R., Tenner, A. J. (2017). Cell-specific deletion of C1qa identifies microglia as the dominant source of C1q in mouse brain. *J Neuroinflammation, 14*, 48. https://doi.org/10.1186/s12974-017-0814-9

Gabanyi, I., Muller, P. A., Feighery, L., Oliveira, T. Y., Costa-Pinto, F. A., Mucida, D. (2016). Neuro-immune interactions drive tissue programming in intestinal macrophages. *Cell, 164*, 378-391. https://doi.org/10.1016/j.cell.2015.12.023

Gattu, S., Bang, Y. J., Pendse, M., Dende, C., Chara, A. L., Harris, T. A., Wang, Y., Ruhn, K. A., Kuang, Z., Sockanathan, S., Hooper, L. V. (2019). Epithelial retinoic acid receptor beta regulates serum amyloid A expression and vitamin A-dependent intestinal immunity. *Proc Natl Acad Sci U S A, 116*, 10911-10916. https://doi.org/10.1073/pnas.1812069116

Grainger, J. R., Konkel, J. E., Zangerle-Murray, T., Shaw, T. N. (2017). Macrophages in gastrointestinal homeostasis and inflammation. *Pflugers Arch, 469*, 527-539. https://doi.org/10.1007/s00424-017-1958-2

Hammond, J. W., Bellizzi, M. J., Ware, C., Qiu, W. Q., Saminathan, P., Li, H., Luo, S., Ma, S. A., Li, Y., Gelbard, H. A. (2020). Complement-dependent synapse loss and microgliosis in a mouse model of multiple sclerosis. *Brain Behav Immun, 87*, 739-750. https://doi.org/10.1016/j.bbi.2020.03.004

Hong, S., Beja-Glasser, V. F., Nfonoyim, B. M., Frouin, A., Li, S., Ramakrishnan, S., Merry, K. M., Shi, Q., Rosenthal, A., Barres, B. A., Lemere, C. A., Selkoe, D. J., Stevens, B. (2016). Complement and microglia mediate early synapse loss in Alzheimer mouse models. *Science, 352*, 712-716. https://doi.org/10.1126/science.aad8373

Johnson, C.D., Barlow-Anacker, A.J., Pierre, J.F., Touw, K., Erickson, C.S., Furness, J.B., Epstein, M.L., Gosain, A. (2018). Deletion of choline acetyltransferase in enteric neurons results in postnatal intestinal dysmotility and dysbiosis. *FASEB J, 32*, 4744–4752. https://doi.org/10.1096/fj.201701474RR

Kishore, U., Reid, K. B. (2000). C1q: structure, function, and receptors. *Immunopharmacology, 49*, 159-170. https://doi.org/10.1016/s0162-3109(00)80301-x

Klindworth, A., Pruesse, E., Schweer, T., Peplies, J., Quast, C., Horn, M., Glockner, F. O. (2013). Evaluation of general 16S ribosomal RNA gene PCR primers for classical and next-generation sequencing-based diversity studies. *Nucleic Acids Res, 41*, e1. https://doi.org/10.1093/nar/gks808

Korb, L. C., Ahearn, J. M. (1997). C1q binds directly and specifically to surface blebs of apoptotic human keratinocytes: complement deficiency and systemic lupus erythematosus revisited. *J Immunol, 158*, 4525-4528. https://www.ncbi.nlm.nih.gov/pubmed/9144462

Kouser, L., Madhukaran, S. P., Shastri, A., Saraon, A., Ferluga, J., Al-Mozaini, M., Kishore, U. (2015). Emerging and novel functions of complement protein C1q. *Front Immunol, 6*, 317. https://doi.org/10.3389/fimmu.2015.00317

Kulkarni, S., Micci, M. A., Leser, J., Shin, C., Tang, S. C., Fu, Y. Y., Liu, L., Li, Q., Saha, M., Li, C., Enikolopov, G., Becker, L., Rakhilin, N., Anderson, M., Shen, X., Dong, X., Butte, M. J., Song, H., Southard-Smith, E. M., Kapur, R. P., Bogunovic, M., Pasricha, P. J. (2017). Adult enteric nervous system in health is maintained by a dynamic balance between neuronal apoptosis and neurogenesis. *Proc Natl Acad Sci USA, 114*, E3709-E3718. https://doi.org/10.1073/pnas.1619406114

Ling, G. S., Crawford, G., Buang, N., Bartok, I., Tian, K., Thielens, N. M., Bally, I., Harker, J. A., Ashton-Rickardt, P. G., Rutschmann, S., Strid, J., Botto, M. (2018). C1q restrains autoimmunity and viral infection by regulating CD8+ T cell metabolism. *Science, 360*, 558-563. https://doi.org/10.1126/science.aao4555

Luo, J., Qian, A., Oetjen, L. K., Yu, W., Yang, P., Feng, J., Xie, Z., Liu, S., Yin, S., Dryn, D., Cheng, J., Riehl, T. E., Zholos, A. V., Stenson, W. F., Kim, B. S., Hu, H. (2018,). TRPV4 channel signaling in macrophages promotes gastrointestinal motility via direct effects on smooth muscle cells. *Immunity, 49*, 107-119 e104. https://doi.org/10.1016/j.immuni.2018.04.021

Macedo, A. C., Isaac, L. (2016). Systemic lupus erythematosus and deficiencies of early components of the complement classical pathway. *Front Immunol, 7*, 55. https://doi.org/10.3389/fimmu.2016.00055

Mao, Y. L., Shen, C. L., Zhou, T., Ma, B. T., Tang, L. Y., Wu, W. T., Zhang, H. X., Lu, H. L., Xu, W. X., Wang, Z. G. (2017). Ablation of Tacr2 in mice leads to gastric emptying disturbance. *Neurogastroenterol Motil, 29*, e13117. https://doi.org/10.1111/nmo.13117

Matheis, F., Muller, P. A., Graves, C. L., Gabanyi, I., Kerner, Z. J., Costa-Borges, D., Ahrends, T., Rosenstiel, P., Mucida, D. (2020). Adrenergic signaling in muscularis macrophages limits infection-induced neuronal loss. *Cell, 180*, 64-78 e16. https://doi.org/10.1016/j.cell.2019.12.002

880
881 Maurer, A. H. (2016). Gastrointestinal motility, part 2: small-bowel and colon transit. *J Nucl Med Technol,*
882 *44*, 12-18. https://doi.org/10.2967/jnumed.113.134551
883
884 Mortazavi, A., Williams, B. A., McCue, K., Schaeffer, L., Wold, B. (2008). Mapping and quantifying
885 mammalian transcriptomes by RNA-Seq. *Nat Methods, 5*, 621-628. https://doi.org/10.1038/nmeth.1226
886
887 Muller, P. A., Koscso, B., Rajani, G. M., Stevanovic, K., Berres, M. L., Hashimoto, D., Mortha, A.,
888 Leboeuf, M., Li, X. M., Mucida, D., Stanley, E. R., Dahan, S., Margolis, K. G., Gershon, M. D., Merad,
889 M., Bogunovic, M. (2014). Crosstalk between muscularis macrophages and enteric neurons regulates
890 gastrointestinal motility. *Cell, 158*, 300-313. https://doi.org/10.1016/j.cell.2014.04.050
891
892 Noris, M., Remuzzi, G. (2013). Overview of complement activation and regulation. *Semin Nephrol, 33*,
893 479-492. https://doi.org/10.1016/j.semnephrol.2013.08.001
894
895 Obata, Y., Castaño, A., Boeing, S., Bon-Frauches, A.C., Fung, C., Fallesen, T., de Agüero, M.G., Yilmaz,
896 B., Lopes, R., Huseynova, A., Horswell, S., Maradana, M.R., Boesmans, W., Vanden Berghe, P., Murray,
897 A.J., Stockinger, B., Macpherson, A.J., Pachnis, V. (2020). Neuronal programming by microbiota regulates
898 intestinal physiology. *Nature, 578*, 284-289. https://doi.org/10.1038/s41586-020-1975-8
899
900 Paloneva, J., Manninen, T., Christman, G., Hovanes, K., Mandelin, J., Adolfsson, R., Bianchin, M., Bird,
901 T., Miranda, R., Salmaggi, A., Tranebjaerg, L., Konttinen, Y., Peltonen, L. (2002). Mutations in two genes
902 encoding different subunits of a receptor signaling complex result in an identical disease phenotype. *Am J*
903 *Hum Genet, 71*, 656-662. https://doi.org/10.1086/342259
904
905 Petry, F., Botto, M., Holtappels, R., Walport, M. J., Loos, M. (2001). Reconstitution of the complement
906 function in C1q-deficient (C1qa-/-) mice with wild-type bone marrow cells. *J Immunol, 167*, 4033-4037.
907 https://doi.org/10.4049/jimmunol.167.7.4033
908
909 Rao, M., Gershon, M. D. (2016). The bowel and beyond: the enteric nervous system in neurological
910 disorders. *Nat Rev Gastroenterol Hepatol, 13*, 517-528. https://doi.org/10.1038/nrgastro.2016.107
911
912 Rolig, A.S., Mittge, E.K., Ganz, J., Troll, J.V., Melancon, E., Wiles, T.J., Alligood, K., Stephens, W.Z.,
913 Eisen, J.S., Guillemin, K. (2017). The enteric nervous system promotes intestinal health by constraining
914 microbiota composition. *PLoS Biol*, 15, e2000689. https://doi.org/10.1371/journal.pbio.2000689
915
916 Schifferli, J. A., Ng, Y. C., Peters, D. K. (1986). The role of complement and its receptor in the elimination
917 of immune complexes. *N Engl J Med, 315*, 488-495. https://doi.org/10.1056/NEJM198608213150805
918
919 Schwechter, B., Rosenmund, C., Tolias, K. F. (2013). RasGRF2 Rac-GEF activity couples NMDA receptor
920 calcium flux to enhanced synaptic transmission. *Proc Natl Acad Sci USA, 110*, 14462-14467.
921 https://doi.org/10.1073/pnas.1304340110
922
923 Shah, D., Romero, F., Zhu, Y., Duong, M., Sun, J., Walsh, K., Summer, R. (2015). C1q deficiency promotes
924 pulmonary vascular inflammation and enhances the susceptibility of the lung endothelium to injury. *J Biol*
925 *Chem, 290*, 29642-29651. https://doi.org/10.1074/jbc.M115.690784
926
927 Thielens, N. M., Tedesco, F., Bohlson, S. S., Gaboriaud, C., Tenner, A. J. (2017). C1q: A fresh look upon
928 an old molecule. *Mol Immunol, 89*, 73-83. https://doi.org/10.1016/j.molimm.2017.05.025

Tian, X. P., Zhang, X. (2010). Gastrointestinal involvement in systemic lupus erythematosus: insight into pathogenesis, diagnosis and treatment. *World J Gastroenterol, 16*, 2971-2977. https://doi.org/10.3748/wjg.v16.i24.2971

Ural, B. B., Yeung, S. T., Damani-Yokota, P., Devlin, J. C., de Vries, M., Vera-Licona, P., Samji, T., Sawai, C. M., Jang, G., Perez, O. A., Pham, Q., Maher, L., Loke, P., Dittmann, M., Reizis, B., Khanna, K. M. (2020). Identification of a nerve-associated, lung-resident interstitial macrophage subset with distinct localization and immunoregulatory properties. *Sci Immunol, 5*. https://doi.org/10.1126/sciimmunol.aax8756

van Schaarenburg, R. A., Suurmond, J., Habets, K. L., Brouwer, M. C., Wouters, D., Kurreeman, F. A., Huizinga, T. W., Toes, R. E., Trouw, L. A. (2016). The production and secretion of complement component C1q by human mast cells. *Mol Immunol, 78*, 164-170. https://doi.org/10.1016/j.molimm.2016.09.001

Vrees, M. D., Pricolo, V. E., Potenti, F. M., Cao, W. (2002). Abnormal motility in patients with ulcerative colitis: the role of inflammatory cytokines. *Arch Surg, 137*, 439-445. https://doi.org/10.1001/archsurg.137.4.439

Warren, J., Mastroeni, P., Dougan, G., Noursadeghi, M., Cohen, J., Walport, M. J., Botto, M. (2002). Increased susceptibility of C1q-deficient mice to Salmonella enterica serovar Typhimurium infection. *Infect Immun, 70*, 551-557. https://doi.org/10.1128/IAI.70.2.551-557.2002

Wessels, M. R., Butko, P., Ma, M., Warren, H. B., Lage, A. L., Carroll, M. C. (1995). Studies of group B streptococcal infection in mice deficient in complement component C3 or C4 demonstrate an essential role for complement in both innate and acquired immunity. *Proc Natl Acad Sci U S A, 92*, 11490-11494. https://doi.org/10.1073/pnas.92.25.11490

Yang, C. H., Yeh, Y. J., Wang, J. Y., Liu, Y. W., Chen, Y. L., Cheng, H. W., Cheng, C. M., Chuang, Y. J., Yuh, C. H., Chen, Y. R. (2017). NEAP/DUSP26 suppresses receptor tyrosine kinases and regulates neuronal development in zebrafish. *Sci Rep, 7*, 5241. https://doi.org/10.1038/s41598-017-05584-7

Yu, X., Rollins, D., Ruhn, K. A., Stubblefield, J. J., Green, C. B., Kashiwada, M., Rothman, P. B., Takahashi, J. S., Hooper, L. V. (2013). TH17 cell differentiation is regulated by the circadian clock. *Science, 342*, 727-730. https://doi.org/10.1126/science.1243884

Yu, X., Wang, Y., Deng, M., Li, Y., Ruhn, K. A., Zhang, C. C., Hooper, L. V. (2014). The basic leucine zipper transcription factor NFIL3 directs the development of a common innate lymphoid cell precursor. *Elife, 3, e04406*. https://doi.org/10.7554/eLife.04406

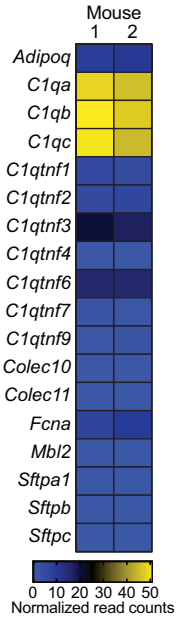

Figure 1 - figure supplement 1. C1q is expressed in the mouse colon.
RNA-seq analysis of soluble defense collagen expression in the colons of C57BL/6 mice. Data were reanalyzed from Gattu et al., 2019. Each column represents one mouse. Data are available in the Gene Expression Omnibus repository under accession number GSE122471.

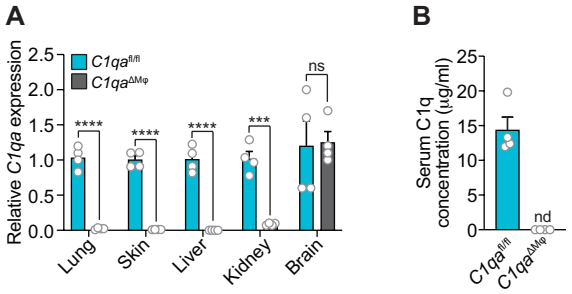

Figure 2 - figure supplement 1. C1q expression is lost systemically but preserved in the central nervous system of *C1qa*$^{\Delta M\varphi}$ mice.

(A) qPCR measurement of *C1qa* expression in lung, skin, liver, kidney, and brain. Each data point represents one mouse. Data are representative of two independent experiments.

(B) C1q is absent from the serum of *C1qa*$^{\Delta M\varphi}$ mice. Enzyme-linked immunosorbent assay (ELISA) detection of serum C1q protein from *C1qa*$^{fl/fl}$ and *C1qa*$^{\Delta M\varphi}$ littermates. Data are presented as C1q serum concentration based on a standard curve generated from purified recombinant mouse C1q. Each data point represents one mouse. nd, not detected. Data are representative of three independent experiments.

Error bars represent SEM. ***p<0.001; ****p<0.0001; ns, not significant by two-tailed Student's t-test.

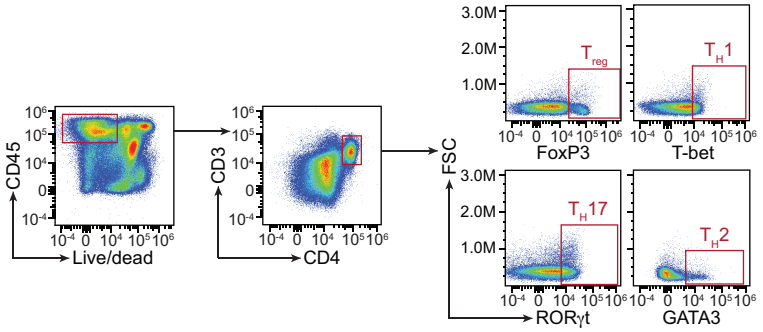

Figure 3 - figure supplement 1. Flow cytometry gating strategy for comparison of T cell populations in *C1qa*$^{fl/fl}$ and *C1qa*$^{\Delta M\varphi}$ mice.

Small intestinal cells were recovered from *C1qa*$^{fl/fl}$ and *C1qa*$^{\Delta M\varphi}$ littermates and analyzed by flow cytometry. T cells were gated as live CD45$^+$ CD3$^+$ CD4$^+$. T cell subsets were further identified by gating into T_{reg} (FoxP3$^+$), T_H1 (T-bet$^+$), T_H17 (RORγt$^+$), and T_H2 (GATA3$^+$). Representative plots from *C1qa*$^{fl/fl}$ mice are presented and comparisons between *C1qa*$^{fl/fl}$ and *C1qa*$^{\Delta M\varphi}$ littermates are shown in Figure 3. FSC, forward scatter.

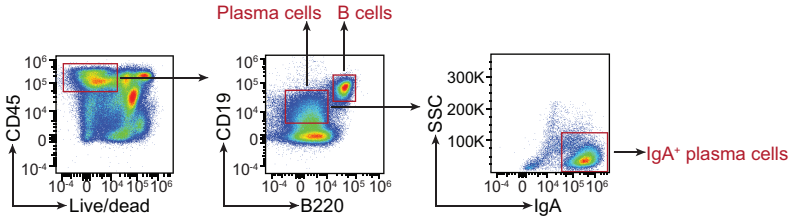

Figure 3 - figure supplement 2. Flow cytometry gating strategy for comparison of B cell and plasma cell populations in *C1qa*$^{fl/fl}$ and *C1qa*$^{\Delta M\varphi}$ mice.

Small intestinal cells were recovered from *C1qa*$^{fl/fl}$ and *C1qa*$^{\Delta M\varphi}$ littermates and analyzed by flow cytometry. B cells were gated as live CD45^{+} CD19^{+} B220^{+}. Plasma cells were gated as CD19^{+} B220^{-}, and IgA^{+} plasma cells were further identified. Representative plots from *C1qa*$^{fl/fl}$ mice are presented and comparisons between *C1qa*$^{fl/fl}$ and *C1qa*$^{\Delta M\varphi}$ littermates are shown in Figure 3. SSC, side scatter.

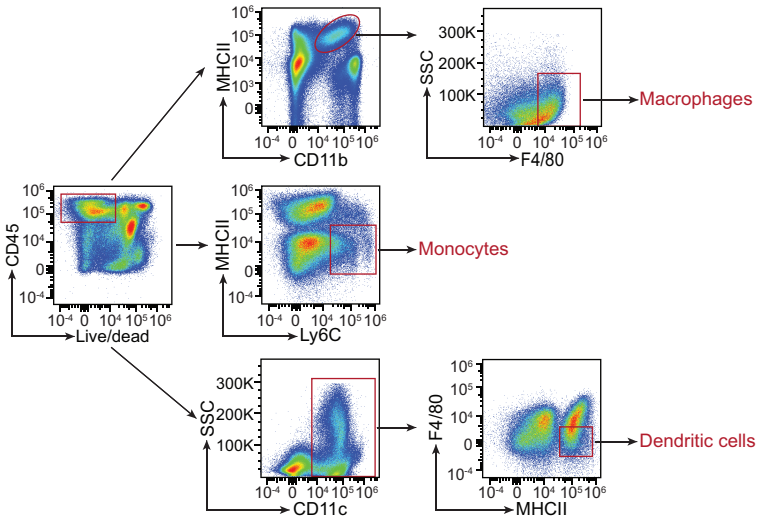

Figure 3 - figure supplement 3. Flow cytometry gating strategy for comparison of myeloid cell populations in *C1qa*$^{fl/fl}$ and *C1qa*$^{\Delta M\varphi}$ mice.

Small intestinal cells were recovered from *C1qa*$^{fl/fl}$ and *C1qa*$^{\Delta M\varphi}$ littermates and analyzed by flow cytometry. Macrophages were gated as live CD45^{+} MHCII^{+} CD11b^{+} F4/80^{hi}. Monocytes were gated as live CD45^{+} MHCII^{-} Ly6C^{+}. Dendritic cells were gated as live CD45^{+} CD11c^{+} MHCII^{+} F4/80^{lo}. Representative plots from *C1qa*$^{fl/fl}$ mice are presented and comparisons between *C1qa*$^{fl/fl}$ and *C1qa*$^{\Delta M\varphi}$ littermates are shown in Figure 3. SSC, side scatter; MHCII, major histocompatibility complex II.

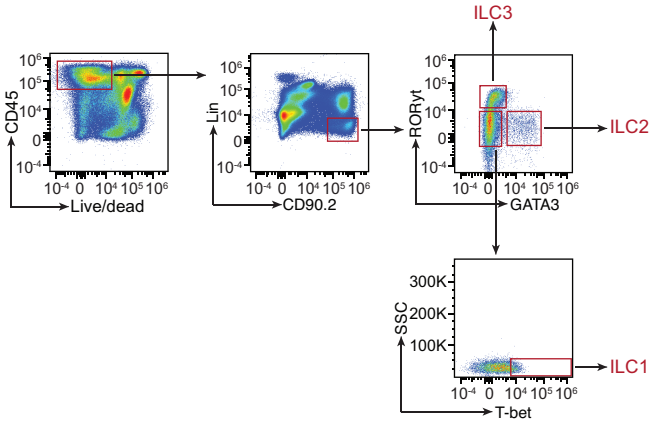

Figure 3 - figure supplement 4. Flow cytometry gating strategy for comparison of innate lymphoid cell populations in *C1qa*$^{fl/fl}$ and *C1qa*$^{\Delta M\varphi}$ mice.

Small intestinal cells were recovered from *C1qa*$^{fl/fl}$ and *C1qa*$^{\Delta M\varphi}$ littermates and analyzed by flow cytometry. Innate lymphoid cells (ILC) were gated as live CD45^{+} Lin^{-} CD90.2^{+} and then further identified as ILC1 (RORγt- GATA3^{-} T-bet^{+}), ILC2 (RORγt^{-} GATA3^{+}) and ILC3 (RORγt^{+} GATA3^{-}). Representative plots from *C1qa*$^{fl/fl}$ mice are presented and comparisons between *C1qa*$^{fl/fl}$ and *C1qa*$^{\Delta M\varphi}$ littermates are shown in Figure 3. SSC, side scatter.

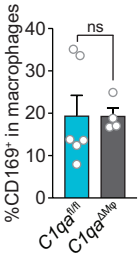

Figure 4 - figure supplement 1. Similar numbers of CD169^{+} macrophages are present in the small intestines of *C1qa*$^{\Delta M\varphi}$ and *C1qa*$^{fl/fl}$ littermates.

Flow cytometry analysis of CD169^{+} macrophages was conducted on cells recovered from the small intestines of *C1qa*$^{\Delta M\varphi}$ and *C1qa*$^{fl/fl}$ littermates. CD169^{+} cells were determined as a percentage of total macrophages (live CD45^{+} CD11b^{+} MHCII^{+} F4/80^{hi} cells).

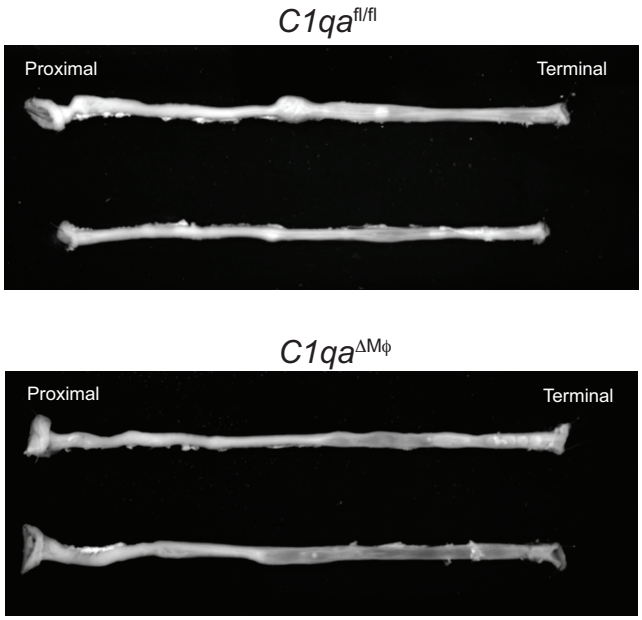

Figure 5 - figure supplements 1 and 2. *Ex vivo* video recordings of colonic peristalsis in *C1qa*$^{fl/fl}$ and *C1qa*$^{\Delta M\varphi}$ littermates.
Still images captured from *ex vivo* video recordings of colonic peristalsis to indicate orientation of the colons. Colons were allowed to equilibrate to the organ chamber for 30 minutes before video recording. Movies were captured over 15 minutes. Colons from *C1qa*$^{fl/fl}$ mice are shown in figure supplement 1; colons from *C1qa*$^{\Delta M\varphi}$ are shown in figure supplement 2.